Proceedings of the Project Review, Geo-Mathematical Imaging Group (Purdue University, West Lafayette IN),
Vol. 1 (2008) pp. 141-163.

VELOCITY CONTINUATION IN THE DOWNWARD CONTINUATION APPROACH TO SEISMIC IMAGING

ANTON A. DUCHKOV* AND MAARTEN V. DE HOOP†

Abstract. One way of developing a wave-equation approach to seismic imaging is based on the concept of downward continuation of the surface reflection data. Seismic imaging is typically based on the single scattering approximation, and assumes the knowledge of a, smooth, background model in which the mentioned downward continuation is carried out. The downward continued data are subjected, at each depth, to an imaging condition generating an image or to an angle transform generating common image-point gathers. In this paper, we develop a general framework for velocity continuation in the downward continuation approach to seismic imaging, motivated by the problem of estimation of the background model. A key aspect of velocity continuation is that the downward continuation of data needs to be carried out only once, namely for an 'initial' background model. Velocity continuation maps these downward continued data to data, downward continued in the 'final' velocity model. We take a broad perspective, leading to a variety of new insights and the development of novel algorithms. To begin with, we will use an extended image, which is a function of subsurface source-receiver midpoint, subsurface source-receiver offset and depth, rather than the traditional image. We base our framework on the double-square-root (DSR) equation, and impose the DSR assumption. We then introduce the concept of data-extended-image 'volume'. In the data-extended-image 'volume', we introduce and analyze velocity continuation of the individual components that make up the process of imaging, migration, and the angle transform: Data continuation nested in velocity continuation, extended image velocity continuation, and image gathers velocity continuation. Each of them can perform a different task for background model, velocity, analysis. The framework presented here extends naturally to applications in time-lapse seismics.

Key words. velocity continuation – imaging – double-square-root equation – reflection tomography

1. Introduction. One way of developing a wave-equation approach to seismic imaging is based on the concept of downward continuation. Surface seismic reflection data, viewed as a function of source, receiver and time, are downward continued into the subsurface to yield virtual seismic reflection data at depth. These are then subjected, at each depth, to an imaging condition generating an image [8] or to an angle transform [10] generating common image-point gathers [35, 37]; see also [11] for the scattered-ray geometry underlying the wave-equation angle transform. Common image-point gathers reflect the redundancy in seismic data and can be exploited in wave-equation reflection tomography [37, 12, 13] or in inverse scattering for reflection coefficients.

Seismic imaging is typically based on the single scattering approximation, and assumes the knowledge of a, smooth, background model in which the above mentioned downward continuation is carried out. Scatterers or reflectors are imaged from reflections in the data. In seismic reflection tomography one aims at determining the background model using the reflections in the data without knowing where the scatterers are. Typically, the reflection tomography is carried out through optimization [39, 13] leading to a sequence of updates in the background model. Through the process of updating, wave-equation reflection tomography meets the notion of velocity continuation. With velocity continuation it is possible to update the image without remigrating the data [15]; we will refer to this paper here as Paper I. In general, velocity continuation admits an efficient way of imaging while sampling the background model space. We note, however, that the evaluation of the operator generating the continuation does typically require retracing rays, dynamically, in changing models.

In this paper, we will take a broad perspective of velocity continuation in the context of downward continuation, leading to a variety of new insights and the development of novel algorithms. To begin with, we will use the extended image, which is a function of subsurface source-receiver midpoint, subsurface source-receiver offset and depth [35, 36], rather than the traditional image. In three dimensions, through the downward continuation, the surface reflection data (at zero depth) and the subsurface extended reflector image (at zero time) are both defined on five-dimensional 'hyperplanes' in a six-dimensional data-extended-image 'volume', which have the source-receiver axes in common. From this volume one can extract 'virtual' subsurface experiments. In the data-extended-image 'volume', we introduce and analyze velocity continuation of the individual components that make up the process of imaging, migration, and the angle transform:

*Center for Computational and Applied Mathemematics, and Geo-Mathematical Imaging Group, Purdue University, West Lafayette, IN 47907, USA (aduchkov@purdue.edu).

†Center for Computational and Applied Mathemematics, and Geo-Mathematical Imaging Group, Purdue University, West Lafayette, IN 47907, USA (mdehoop@purdue.edu).

Data continuation in depth nested in velocity continuation, extended image velocity continuation, and image gather velocity continuation. Each of them can perform a different task for background model, velocity, analysis. This background model analysis can naturally extend to applications in time-lapse seismics.

The velocity continuation is, in all cases considered, accomplished by solving an evolution equation (Paper I). In this paper, the downward continuation is based on the double-square-root (DSR) equation [6, 9, 8], which is intimately connected to the one-way wave equation [8, 17, 18]. We use techniques from microlocal analysis, in particular Egorov's theorem, to construct the evolution operator corresponding with the different types of velocity continuation. The key assumption for the construction to apply is the so-called DSR condition: The rays are nowhere horizontal, that is, energy propagates nowhere horizontally.

In our analysis, it is fundamental to consider extended images and image gathers rather than traditional images. Velocity continuation is built from 'invertible' operators. A straightforward dimension check, in three dimensions, reveals that reflection seismic data are five-dimensional while a traditional image is three-dimensional. Indeed, the extension of the image while matching the dimensions of the data results in the required 'invertibility' (of the time-to-depth conversion operator [37]) even in the presence of caustics.

The notion of velocity continuation is, through the evolution equation, closely connected to perturbation theory. Indeed, perturbation arguments can aid in the construction of the above mentioned evolution operator. For example, perturbed, or sometimes referred to as 'residual', downward continuation under velocity perturbation is essentially velocity continuation of data continuation in depth, from an initial model to a perturbed model.

The literature on image continuation [19, 21, 23, 25, 1, 27, 29] was discussed in Paper I. In Paper I, we introduced a general framework for continuation, while in this paper we consider specifically velocity continuation through data downward continuation with the DSR equation. (The idea of combining data continuation, namely, transformation to zero source-receiver offset, with velocity continuation was already used in [2, 3].) The perturbation of downward continuation can be derived from the perturbation of the double-square-root operator [32, 12, 13], reminiscent of a generalized screen expansion of the square-root operator [26]. Continuation operators are solution operators to evolution equations (Paper I). They propagate singularities ('fronts') in accordance with ray theory associated with a Hamiltonian standardly obtained as the principal symbol of the evolution operator. Ray perturbation theory [16] has been used as a tool to construct such continuation 'rays', without finding a Hamiltonian, for the purpose of image continuation [1, 25]. The Hamiltonian we construct here for velocity continuation of downward continuation, valid in heterogeneous models, reduces in homogeneous models to a form which is related to formulas obtained in [21, 31]. Velocity continuation of data downward continuation appears in the development of downward-continuation based wave-equation migration velocity analysis (MVA): One can construct annihilators of the data [35] that generalize the notion of differential semblance [39] and that can be used to carry out the MVA through optimization [12, 32, 33, 13]. The construction of these annihilators is intimately connected to the generation of image gathers through the above mentioned angle transform that is derived from downward continuation [37].

First, we summarize the results of Paper I which pertain to velocity continuation. In Section 3, we discuss and analyze the evolution equations that describe data continuation in depth (Subsection 3.1), and data continuation in two-way traveltime (Subsection 3.2), both making use of the DSR equation. Data continuation in two-way time aids in developing an understanding of the above mentioned six-dimensional data-extended-image volume; in particular, for background velocity models that vary in depth only, one can recover the evolution equation associated with the exploding reflector model. We also extend the notion of isochron rays, namely, to the ones associated with the extended image. In Section 4, we develop velocity continuation of downward continued data, and construct the associated continuation rays in phase space (Subsection 4.2). In Section 5 we introduce the velocity continuation of extended images (Subsection 5.1) and of common image-point gathers (Subsection 5.2). The relevant derivations and constructions make use of Egorov's theorem, which is described in Appendix A. In Section 6 we present a numerical example of image continuation and continuation of common image-point gathers. Synthetic model includes a lens generating caustics in the background models and a horizontal reflector. In Section 7, we construct evolution operators for the different types of velocity continuation in homogeneous velocity models, in closed form. These are used to illustrate the basic concepts, and recover, for example, the equations for residual Stolt migration [38]. In Appendix B

we provide the evolution equations for velocity continuation of data downward continuation and extended image velocity continuation in background velocity models that vary in depth only, in particular the case of constant gradients. We conclude with a discussion.

2. Velocity continuation. A comprehensive framework of continuation of seismic data and images was introduced in Paper I. Here, we summarize some key aspects of the theory developed there that apply to velocity continuation. To facilitate the introduction of velocity continuation, we consider a one-parameter family, $c(\alpha)$, of velocity models. This family can be viewed as a curve or trajectory in a space of allowable models. Optimization in wave-equation reflection tomography would yield samples of models on such a curve. Let $w(\alpha, X)$ denote downward continued data, an image, or image gathers, evaluated with model $c(\alpha)$, whereas X stands for the coordinates of the space on which $w(\alpha, .)$ is defined; α will be referred to as the evolution parameter.

Continuation operators. An operator $C_{(\alpha,\alpha_0)}$ is a continuation operator if it transforms $w(\alpha_0, .)$ into $w(\alpha, .)$, that is

$$C_{(\alpha,\alpha_0)} : \; w(\alpha_0, .) \to w(\alpha, .) \tag{2.1}$$

and satisfies the conditions

$$\begin{array}{l} - \; C_{(\alpha_0,\alpha_0)} = \mathsf{Id} \text{ (identity operator);} \\ - \; C_{(\alpha,\alpha_0)} \text{ is invertible,} \end{array} \tag{2.2}$$

for each $\alpha_0, \alpha \in J$, where $J = [\alpha_1, \alpha_2]$ is a given interval. In essence, properties (2.2) imply that $C_{(\alpha,\alpha_0)}$ is a propagator. Indeed, for $\alpha_0 \le \alpha' \le \alpha$ we have $C_{(\alpha,\alpha_0)} = C_{(\alpha,\alpha')} C_{(\alpha',\alpha_0)}$, and α mimics time as in wave propagation. The second condition in (2.2) states that the process of continuation can be reversed.

Evolution equation. With conditions (2.2) and some additional weak assumption, a continuation operator $C_{(\alpha,\alpha_0)}$ is the solution operator to an evolution equation, that is, $w(\alpha, .) = C_{(\alpha,\alpha_0)} w(\alpha_0, .)$ is the solution to the initial value problem

$$[\partial_\alpha - \mathrm{i} P(\alpha, X, D_X)] w(\alpha, X) = 0, \; w|_{\alpha=\alpha_0} = w(\alpha_0, .), \tag{2.3}$$

where $D_X = -\mathrm{i}\partial_X$ are differentiation operators with respect to coordinates X, in dimension n say. Sometimes, we will use the shorthand notation $P = P(\alpha)$. P is a pseudodifferential operator of order 1; the proof of its existence and a construction can be found in Paper I. Basically, the action of P on w is given by

$$P(\alpha, X, D_X) w(\alpha, X) = \frac{1}{(2\pi)^n} \iint P(\alpha, X, \Xi) \, \mathrm{e}^{\mathrm{i}\langle \Xi, X - Y \rangle} w(\alpha, Y) \, \mathrm{d}Y \mathrm{d}\Xi, \tag{2.4}$$

where $P(\alpha, X, \Xi)$ is the operator's symbol which is obtained from $P(\alpha, X, D_X)$ upon replacing D_X by Ξ. Certain mathematical details that pertain to velocity continuation with the double-square-root equation are omitted here; the double-square-root operator is not a pseudodifferential operator globally, but with the introduction of a judiciously chosen damping term, the methods developed here still apply.

Continuation rays. The solution operator of (2.3), that is, the continuation operator, propagates singularities along rays in phase space. These rays are solutions of the Hamilton-Jacobi equations derived from the Hamiltonian

$$\mathcal{H} = \mathcal{H}(\alpha, X, \xi_\alpha, \Xi) = \xi_\alpha - P_1(\alpha, X, \Xi), \tag{2.5}$$

where P_1 is the principal ('high-frequency') symbol of operator P. The Hamilton-Jacobi equations are given by

$$\begin{array}{rclcrcl} \dfrac{\mathrm{d}X}{\mathrm{d}\alpha} & = & \partial_\Xi \mathcal{H} = -\partial_\Xi P_1 & , & \dfrac{\mathrm{d}\Xi}{\mathrm{d}\alpha} & = & -\partial_X \mathcal{H} = \partial_X P_1, \\ & & & & \dfrac{\mathrm{d}\xi_\alpha}{\mathrm{d}\alpha} & = & -\partial_\alpha \mathcal{H} = \partial_\alpha P_1, \end{array} \tag{2.6}$$

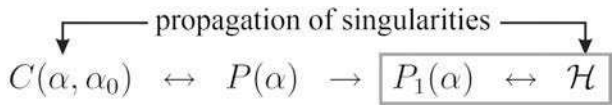

FIG. 1. *Propagation of singularities the continuation operator (2.1) is governed by the evolution operator (2.4) via its principal symbol, and the Hamiltonian (2.5).*

and are supplemented with initial conditions $X(\alpha_0) = X_0$, $\Xi(\alpha_0) = \Xi_0$, $\xi_\alpha(\alpha_0) = \xi_{\alpha 0}$. Note that the top equations do not depend on ξ_α and thus can be solved independently from the bottom equation. The solutions of (2.6) are also written as $X = X(\alpha, \alpha_0, X_0, \Xi_0)$, $\Xi = \Xi(\alpha, \alpha_0, X_0, \Xi_0)$, $\xi_\alpha = \xi_\alpha(\alpha, \alpha_0, X_0, \Xi_0, \xi_{\alpha 0})$ [1]. A diagram emphasizing the interrelation between the continuation operator, the evolution operator, and the underlying geometry and their high-frequency behavior is given in Fig. 1.

To facilitate the introduction of downward continuation, we write the coordinates in space as (z, x), where z denotes depth and x the lateral coordinates. In general, the velocities $c(\alpha) = c(\alpha; z, x)$ will be defined by a representation of the type,

$$c(\alpha; z, x) = \sum_{i \in I} k_i(\alpha)\varphi_i(z, x), \tag{2.7}$$

where the φ_i are basis functions with properties that are desirable (such as compression [28]) for the velocity analysis problem at hand; I is a finite index set.

3. Evolution equations in seismic migration. In this section, we discuss operators for seismic data continuation derived from the double-square-root (DSR) equation. The data are, implicitly, modelled in the single scattering approximation. We assume that the DSR assumption holds, that is, energy propagates nowhere horizontally (cf. [36]). Then the data can be modelled with the DSR equation. We consider both data continuation in depth, z, which arises naturally in imaging, and data continuation in two-way traveltime, t, which arises naturally in modelling. The further analysis will be entirely based on the associated continuation operators. We reserve the symbol u for 'data'; u is a function of depth, z, lateral source coordinates, s, lateral receiver coordinates, r, and time, t. Thus, $u(z = 0, s, r, t) = u_0(s, r, t)$ denotes observed reflection seismic data. The maximum depth considered is Z.

3.1. Data continuation in depth. For upward continuation (used in modelling) the initial value problem takes the form (cf. [36]):

$$(-)[\partial_z - \mathrm{i}P^{DSR}(z, s, r, D_s, D_r, D_t)]u = 0, \quad u(z_1, s, r, t) = u_1(s, r, t); \tag{3.1}$$

this equation is solved in the direction of decreasing z (upward, and forward in time) with initial condition defined at some large depth, z_1 say, at the bottom of the model. The DSR operator P^{DSR} has principal symbol,

$$P_1^{DSR}(z, s, r, \xi_s, \xi_r, \tau) = \tau\sqrt{\frac{1}{c(z,s)^2} - \frac{\|\xi_s\|^2}{\tau^2}} + \tau\sqrt{\frac{1}{c(z,r)^2} - \frac{\|\xi_r\|^2}{\tau^2}}, \tag{3.2}$$

while considering $\tau > 0$. Here, τ denotes frequency and ξ denotes horizontal wave vectors, ξ_s associated with s and ξ_r associated with r. The upward continuation operator, $H_{(z,z_1)} \equiv C^{DSR}_{(z,z_1)}$, with $z < z_1$, is the solution operator of (3.1), that is, $u(z, .) = H_{(z,z_1)}u_1$. (As compared with (2.3) we have $\alpha = z$ and $X = (s, r, t)$.)

[1] In Goldin's (1998) formulation of continuation, for each α, $(X(\alpha, \alpha_0, X_0, \Xi_0), \Xi(\alpha, \alpha_0, X_0, \Xi_0)/\|\Xi(\alpha, \alpha_0, X_0, \Xi_0)\|)$ is identified with a contact element. In image continuation, for example, $X(\alpha; X_0, \Xi_0)$ represents an image point corresponding with a reflector, while the direction of $\Xi(\alpha; X_0, \Xi_0)$ defines the normal to the reflector.

The adjoint, $H^*_{(0,z)}$, of $H_{(0,z)}$ appears to be a solution operator to the initial value problem,

$$[\partial_z - \mathrm{i}P^{DSR}(z,s,r,D_s,D_r,D_t)]u = 0, \quad u(0,s,r,t) = u_0(s,r,t), \tag{3.3}$$

now to be solved in the direction of increasing z (downward, and backward in time) with initial condition defined at the surface. We have $u(z,.) = H^*_{(0,z)}u_0$. We note that we have omitted non-selfadjoint contributions to P^{DSR}; indeed, we have ignored evanescent waves. Then the following property is true:

$$H_{(\bar{z},z)}(\alpha)\ H^*_{(\bar{z},z)}(\alpha) \sim \mathrm{Id}. \tag{3.4}$$

and we will substitute this composition instead of identity operator while deriving different types of evolution operators for velocity continuation further in the text.

Using (2.5) we obtain Hamiltonians for the DSR rays in phase space using depth as the evolution parameter:

$$\mathcal{H}^{DSR}(z,s,r,\xi_z,\xi_s,\xi_r,\tau) = \pm(\xi_z - P_1^{DSR}(z,s,r,\xi_s,\xi_r,\tau)), \tag{3.5}$$

in which the upper signs correspond with downward continuation and the lower signs corresponds with upward continuation. Integrating the Hamilton-Jacobi equations (cf. (2.6)) associated with upward continuation (cf. (3.1)) yields solutions

$$\begin{aligned}(s(z,z_1,\Gamma_1), r(z,z_1,\Gamma_1), t(z,z_1,\Gamma_1), \xi_s(z,z_1,\Gamma_1), \xi_r(z,z_1,\Gamma_1), \tau(z,z_1,\Gamma_1)),\\ \Gamma_1 \equiv (s_1,r_1,t_1,\xi_{s1},\xi_{r1},\tau_1)\end{aligned} \tag{3.6}$$

that define a mapping

$$\Sigma(z,z_1):\ \Gamma_1 \to (\underbrace{s(z,z_1,\Gamma_1), r(z,z_1,\Gamma_1), t(z,z_1,\Gamma_1)}_{\Sigma_1(z,z_1)(\Gamma_1)}, \underbrace{\xi_s(z,z_1,\Gamma_1), \xi_r(z,z_1,\Gamma_1), \tau(z,z_1,\Gamma_1)}_{\Sigma_2(z,z_1)(\Gamma_1)}). \tag{3.7}$$

Modelling. Seismic reflection data, in Born approximation, can be modelled with an inhomogeneous DSR equation [36]:

$$(-)[\partial_z - \mathrm{i}P^{DSR}(z,s,r,D_s,D_r,D_t)]u = R(z,s,r,t), \quad u|_{z=Z} = 0, \tag{3.8}$$

where

$$R(z,s,r,t) = \delta(t)\delta(r-s)\tfrac{1}{2}(c^{-3}\delta c)\left(z, \tfrac{1}{2}(r+s)\right); \tag{3.9}$$

$\delta c(z,x)$ is the function containing the rapid velocity variations representative of the scatterers, superimposed on a smooth background model $c(z,x)$ (which will be parametrized by α). The data are then modelled by the solution at $z=0$: $u(z=0,s,r,t)$.

In the further analysis, it appears useful to transform coordinates from subsurface lateral source and receiver to subsurface midpoint and offset,

$$x = \tfrac{1}{2}(r+s), \quad h = \tfrac{1}{2}(r-s); \tag{3.10}$$

with the transformation

$$\xi_s = \tfrac{1}{2}(\xi_x - \xi_h), \quad \xi_r = \tfrac{1}{2}(\xi_x + \xi_h). \tag{3.11}$$

This coordinate transform can be applied to the symbol of the DSR operator [34, , Thm. 4.2] getting for (subsurface) midpoint and offset, and time coordinates:

$$P^{DSR}(z,x,h,\xi_x,\xi_h,\tau) = P^{DSR}(z,s(x,h),r(x,h),\xi_s(\xi_x,\xi_h),\xi_r(\xi_x,\xi_h),\tau). \tag{3.12}$$

REMARK (offset plane waves). We consider the situation where ξ_h is preserved along all DSR rays, that is, $\frac{\mathrm{d}\xi_h}{\mathrm{d}z} = 0$ along these rays. This holds, in particular, in the case of a vertically inhomogeneous medium, $c = c(z)$. We downward continue, in such a $c(z)$ background model, independently every subset of the data corresponding to a constant value of ξ_h:

$$[\partial_z - \mathrm{i}P^{DSR}(z,x,h,D_x,\xi_h,D_t)]\hat{u} = 0, \quad \hat{u}(z,x,\xi_h,t)|_{z=0} = \hat{u}_0(x,\xi_h,t), \tag{3.13}$$

cf. (3.12), where $\hat{u}$ denotes the Fourier transform of u with respect to h. The principal symbol of the evolution operator can be written in the form (cf. (3.5) subject to coordinate transformation (3.10)-(3.11)):

$$P_1^{DSR}(z,x,h,\xi_x,\xi_h,\tau) = \tau\sqrt{\frac{1}{\widehat{c}(z)^2} - \frac{\|\xi_x\|^2 + 2\langle\xi_h,\xi_x\rangle}{\tau^2}} + \tau\sqrt{\frac{1}{\widehat{c}(z)^2} - \frac{\|\xi_x\|^2 - 2\langle\xi_h,\xi_x\rangle}{\tau^2}}, \tag{3.14}$$

in which $\widehat{c}(z)^{-2} = c(z)^{-2} - \|\xi_h\|^2\tau^{-2}$. The operator with principal symbol (3.14) was introduced in [22] for so-called pre-stack offset plane wave migration. If the term, $2\langle\xi_h,\xi_x\rangle$, is omitted, then the operator in (3.14) reduces to a zero (source-receiver) offset migration (see also (3.23)), with modified velocity given by $\widehat{c}(z)$, for each ξ_h [30].

3.2. Data continuation in two-way traveltime. We discuss an alternative form of data continuation, namely in two-way traveltime rather than depth. Let, for given (z,s,r,ξ_s,ξ_r), Θ denote the mapping $\tau \to \xi_z = P_1^{DSR}(z,s,r,\xi_s,\xi_r,\tau)$. Then Θ^{-1} is the mapping that solves the equation (cf. (3.5))

$$\xi_z = P_1^{DSR}(z,s,r,\xi_s,\xi_r,\Theta^{-1}(z,s,r,\xi_z,\xi_s,\xi_r));$$

it follows that

$$\Theta^{-1}(z,s,r,\xi_z,\xi_s,\xi_r) = \frac{c_r c_s}{|c_{s-r}^2|}\xi_z\sqrt{c_{s+r}^2 + \xi_z^{-2}(\|\xi_r\|^2 - \|\xi_s\|^2)\,c_{s-r}^2 - 2\sqrt{c_s^2c_r^2 + \xi_z^{-2}(\|\xi_r\|^2c_r^2 - \|\xi_s\|^2c_s^2)\,c_{s-r}^2}}, \tag{3.15}$$

which also defines the principal symbol, $P_1^{TWT} = P_1^{TWT}(s,r,z,\xi_s,\xi_r,\xi_z)$ (homogeneous of degree 1 in (ξ_s,ξ_r,ξ_z)) of a pseudodifferential operator P^{TWT} of order 1. Here, $c_r = c(z,r)$, $c_s = c(z,s)$, $c_{s-r}^2 = c(z,s)^2 - c(z,r)^2$ and $c_{s+r}^2 = c(z,s)^2 + c(z,r)^2$. Note that this representation admits the limit $c_{s-r}^2 \to 0$ to be taken:

$$\lim_{c_{s-r}^2\to 0} P_1^{TWT} = \frac{c}{2}\xi_z\sqrt{1 + 2\frac{\|\xi_s\|^2 + \|\xi_r\|^2}{\xi_z^2} + \frac{(\|\xi_s\|^2 - \|\xi_r\|^2)^2}{\xi_z^4}}, \quad 2c^2 = \lim_{c_{s-r}^2\to 0} c_{s+r}^2. \tag{3.16}$$

We consider the mapping

$$h(s,r,z) \to \widetilde{u}(z,s,r,t) = \int_z^Z H_{(z,z')}\delta(t')h\,\mathrm{d}z' = \int\left\{\int_0^Z\!\!\iint \left(H_{(z,z')}\right)(s,r,t,s',r',t')\delta(t')h(s',r',z')\,\mathrm{d}s'\mathrm{d}r'\mathrm{d}z'\right\}\mathrm{d}t'. \tag{3.17}$$

We note that, with $h(s,r,z) = \delta(r-s)\frac{1}{2}(c^{-3}\delta c)\left(z,\frac{1}{2}(r+s)\right)$, $\widetilde{u}(z=0,s,r,t)$ models the data as in (3.8) (cf. [36]). It follows that, up to leading order, $\widetilde{u}(z,s,r,t)$ solves the initial value problem

$$[\partial_t - \mathrm{i}P^{TWT}(s,r,z,D_s,D_r,D_z)]\widetilde{u} = 0, \tag{3.18}$$

supplemented with initial values $\widetilde{u}(z,s,r,0) = h(s,r,z)$ at $t=0$, to be solved in the direction of increasing t (thus decreasing z). In a similar manner we can construct a backward (hence downward) evolution equation

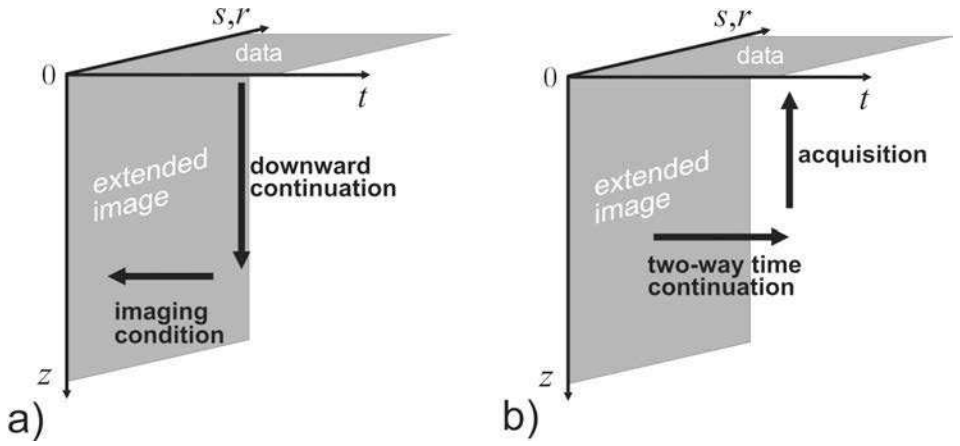

FIG. 2. *Continuation in data-extended-image volume. (a) Downward continuation concept for migration; (b) Two-way traveltime continuation (exploding reflector) concept for demigration.*

and the principal symbol of the evolution operator. (As compared with (2.3) we have $\alpha = t$ and $X = (z, s, r)$.)

Using (2.5) we obtain (time-independent) Hamiltonians for the DSR rays in phase space using time as the evolution parameter:

$$\mathcal{H}^{TWT}(z, s, r, \tau, \xi_z, \xi_s, \xi_r) = \pm(\tau - P_1^{TWT}(z, s, r, \xi_z, \xi_s, \xi_r)), \tag{3.19}$$

in which the upper sign corresponds with forward in time (upward) continuation and the lower sign corresponds with backward in time (downward) continuation.

Transforming coordinates from (subsurface) lateral source and receiver to (subsurface) midpoint and offset, as in (3.10), the principal symbol of P^{TWT} reads

$$P_1^{TWT}(z, x, h, \xi_z, \xi_x, \xi_h) = \tag{3.20}$$
$$\frac{c_r c_s}{|c_-^2|}\xi_z \sqrt{c_+^2 + \xi_z^{-2}\langle \xi_x, \xi_h\rangle\, c_-^2 - \sqrt{4c_s^2 c_r^2 - \xi_z^{-2}(\|\xi_x\|^2 + \|\xi_h\|^2)\,(c_-^2)^2 + 2\xi_z^{-2}\langle \xi_x, \xi_h\rangle c_+^2 c_-^2}},$$

where $c_s = c(z, x-h)$, $c_r = c(z, x+h)$, $c_-^2 = c(z, x-h)^2 - c(z, x+h)^2$, and $c_+^2 = c(z, x-h)^2 + c(z, x+h)^2$.

Equation (3.18) can be used to generalize the notion of exploding reflectors (see remark below), in the data-extended-image volume with coordinates (z, s, r, t) – subject to the extension of reflectivity [36]. The concept of data-extended-image volume that emerged in this section is schematically illustrated in Fig. 2. By continuing surface reflection data, observed at $z = 0$, in depth one fills up the volume with $u = u(z, s, r, t)$. To obtain an extended image, one applies an imaging condition, which amounts to extracting u at the $t = 0$ 'hyperplane' (Fig. 2 (a)). Alternatively, one can consider an extended image, or reflectivity, as a source acting at two-way time $t = 0$, that is subjected to forward continuation in two-way time which also results in filling up the volume, now with $\widetilde{u} = \widetilde{u}(z, s, r, t)$. To recover single scattered data, one extracts $\widetilde{u}$ at the $z = 0$ 'hyperplane' (Fig. 2 (b)).

Vertically inhomogeneous models. In the case of a vertically inhomogeneous velocity model, we have $c(z, r) = c(z, s) = c(z)$. We could use the expressions above, but it is more straightforward to rederive the Hamiltonians directly from (3.5) and (3.2), in s, r coordinates,

$$\mathcal{H}^{TWT}(z, s, r, \tau, \xi_z, \xi_s, \xi_r) = \pm\left(\tau - \xi_z \frac{c(z)}{2}\sqrt{\xi_z^{-4}(\|\xi_s\|^2 - \|\xi_r\|^2)^2 + 2\xi_z^{-2}(\|\xi_r\|^2 + \|\xi_s\|^2) + 1}\right) \tag{3.21}$$

(the analogue of (3.15)) and in x, h coordinates,

$$\mathcal{H}^{TWT}(z,x,h,\tau,\xi_z,\xi_x,\xi_h) = \pm\left(\tau - \xi_z\frac{c(z)}{2}\sqrt{\xi_z^{-4}\langle\xi_x,\xi_h\rangle^2 + \xi_z^{-2}(\|\xi_x\|^2+\|\xi_h\|^2)+1}\right) \tag{3.22}$$

(the analogue of (3.20)). We note that for constant background velocity, $c(z) = v$, equation (3.21) reduces to [31, (3)]; equation (3.22) reduces to the Fourier domain counterpart of [21, (A-10)].

REMARK (exploding reflectors). We use the Hamiltonians for data continuation in two-way traveltime and depth to revisit the exploding reflector model used in the early development of seismic imaging. For a vertically inhomogeneous velocity model, $c(z)$, the Hamiltonian $\mathcal{H}^{TWT}$ in (3.22) does not depend on h, and thus the phase variable ξ_h remains constant in the course of downward continuation ($\frac{\mathrm{d}\xi_h}{\mathrm{d}t} = -\partial_h\mathcal{H}^{TWT} = 0$). For zero source-receiver offset (ZO) surface data, $\xi_h = 0$ (this follows immediately from the symmetry of common midpoint gathers) and it remains zero for all t. Then equation (3.22) reduces to the Hamiltonian for zero-offset data modelling in 'exploding reflector' approach [8, 7]:

$$\tau - \xi_z\frac{c(z)}{2}\sqrt{1+\|\xi_x\|^2\xi_z^{-2}} = \mathcal{H}^{ZO}(x,z,\tau,\xi_x,\xi_z), \tag{3.23}$$

where we recognize the 'half-velocity' $\frac{1}{2}c(z)$ typical for the 'exploding reflector' model. We note that we describe, here, the 'exploding reflector' model by a *first*-order evolution equation instead of a *second*-order wave equation.

REMARK (extended isochron rays). The principal symbol given in (3.20) can be used to form forward and backward Hamiltonians, $\mathcal{H}^{TWT}$, as in (3.19), and set up corresponding Hamilton-Jacobi equations. Their solutions,

$$(z(t,t_0,\Gamma_0),x(t,t_0,\Gamma_0),h(t,t_0,\Gamma_0),\xi_z(t,t_0,\Gamma_0),\xi_x(t,t_0,\Gamma_0),\xi_h(t,t_0,\Gamma_0)), \quad \Gamma_0 \equiv (z_0,x_0,h_0,\xi_{z0},\xi_{x0},\xi_{h0}), \tag{3.24}$$

are continuation rays in phase space. The frequency, τ, is constant along the rays; in particular,

$$\mathcal{H}^{TWT}(z_0,x_0,h_0,\tau,\xi_{z0},\xi_{x0},\xi_{h0}) = 0. \tag{3.25}$$

We consider the backward propagation it time from $t = t_0$ to 0. For each fixed point, (z_0,x_0,h_0), the above mentioned solutions generate a hypersurface,

$$(z(0,t_0,\Gamma_0),x(0,t_0,\Gamma_0),h(0,t_0,\Gamma_0)),$$

in the extended image space with coordinates (z,x,h). This hypersurface is parametrized through $(\xi_{z0},\xi_{x0},\xi_{h0})$ subject to constraint (3.25). If $z_0 = 0$, the above mentioned hypersurface may be regarded as an extension of the notion of isochron. Isochrons in seismic imaging form the 'impulse response' of the imaging operator, that is, they are the fronts in image space that originate from a particular data sample.

For the case of a constant (unit) velocity model, some extended isochrons are shown in Fig. 3 (a). The three hypersurfaces correspond with $(z_0,x_0,h_0) = (0,0,.5)$ and the two-way time, t_0, is set to 1, 3 and 5. The conventional isochrons follow from intersecting the extended isochrons with the $h = 0$ hyperplane in the extended image space (the thick grey lines in Fig. 3 (b), for $t_0 = 3$ and 5). We note that extended isochrons exist for every $t_0 \geq 0$, while they will not intersect the $h = 0$ hyperplane for sufficiently small t_0. Indeed, conventional isochrons do not exist for $t_0 < 1$ in the model example shown in Fig. 3 (b).

Extended isochron rays are described by (3.24) subject to setting time $t = 0$. These rays have t_0 as evolution parameter:

$$(z(0,t_0,\Gamma_0),x(0,t_0,\Gamma_0),h(0,t_0,\Gamma_0),\xi_z(0,t_0,\Gamma_0),\xi_x(0,t_0,\Gamma_0),\xi_h(0,t_0,\Gamma_0)). \tag{3.26}$$

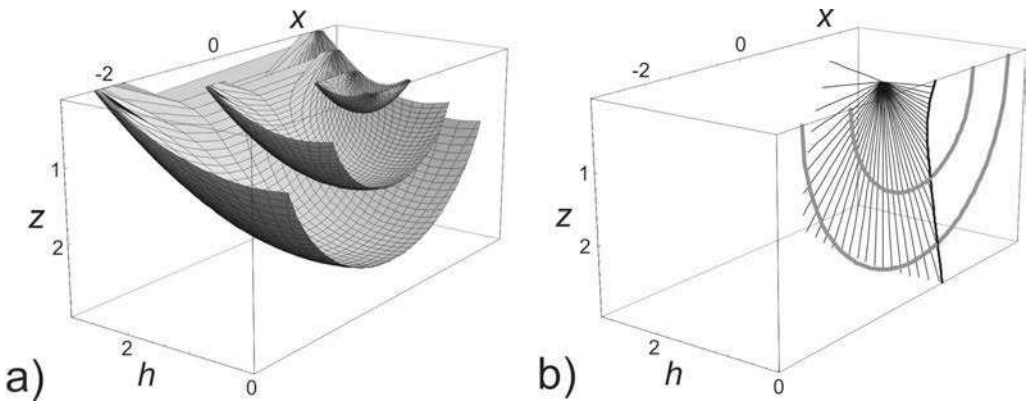

FIG. 3. *Notion of isochrons. (a) Extended isochrons for two-way traveltimes $t = 1, 3, 5$; (b) Conventional isochrons (thick grey lines) and isochron rays (thick black lines) in the image space obtained by intersection of the extended isochrons and rays with the $h = 0$ hyperplane.*

We now establish the connection between extended isochron rays (3.26) and isochron rays for common (source-receiver) offset migration as defined in [24]. Fig. 3 (b) provides some intuition about their construction. We consider an n-dimensional configuration ($n = 2, 3$). We fix $(z_0 = 0, x_0, h_0)$, but, naturally, not t_0. As noticed above, equation (3.26) generates a $(2n-2)$-dimensional 'fan' of rays parametrized through $(\xi_{z0}, \xi_{x0}, \xi_{h0})$ which is $(2n-1)$-dimensional set but we loose one dimension due to constraint (3.25). The 'common offset' restriction is enforced by fixing ξ_{x0} (this value is constrained by common-offset data), whence the 'fan' of rays becomes $(n-1)$-dimensional, and will be parametrized through (ξ_{z0}, ξ_{h0}), again, subject to constraint (3.25). The points where these rays (indicated by thin black lines in Fig. 3 (b)) intersect the $h = 0$ hyperplane lie precisely on a conventional isochron ray (the thick black line in Fig. 3 (b)).

In [24] the isochron rays are parametrized by t_0. Under certain assumptions, we can recover this parametrization from our construction. Again, we fix $(z_0 = 0, x_0, h_0)$ and ξ_{x0}. For each t_0, we need to find a (ξ_{h0}, ξ_{z0}) such that constraint (3.25) is satisfied and that the extended isochron ray in (3.26) precisely reaches the $h = 0$ hyperplane. That is,

$$h(0, t_0, \Gamma_0) = 0 \quad \text{for } \Gamma_0 = (z_0 = 0, x_0, h_0, \xi_{z0}, \xi_{x0}, \xi_{h0}). \tag{3.27}$$

If a solution exists, we write it as $(\xi_{z0}(t_0, x_0, h_0, z_0 = 0, \xi_{x0}), \xi_{h0}(t_0, x_0, h_0, z_0 = 0, \xi_{x0}))$. The conventional isochron rays (in the 'combined parametrization' [24]) follow to be

$$(z(0, t_0, \Gamma_0), x(0, t_0, \Gamma_0)), \qquad \Gamma_0 = (z_0, x_0, h_0, \xi_{z0}(t_0, x_0, h_0, z_0 = 0, \xi_{x0}), \xi_{0x}, \xi_{h0}(t_0, x_0, h_0, z_0 = 0, \xi_{x0})). \tag{3.28}$$

To recover a Hamiltonian from these expressions, see Paper I.

4. Velocity continuation of downward continued data. In this section, we apply the notion of velocity continuation to data downward continuation. To this end, we reconsider the smooth family of background velocity models, $c(\alpha; z, x)$, depending on a parameter α. The initial value problem (3.3) for downward continuation is modified to depend smoothly on α:

$$[\partial_z - \mathrm{i}P^{DSR}(\alpha; z, s, r, D_s, D_r, D_t)]u(\alpha; .) = 0, \quad u(\alpha; 0, s, r, t) = u_0(s, r, t), \tag{4.1}$$

in which the principal symbols of the one-parameter family of DSR operators,

$$P^{DSR}(\alpha) = P^{DSR}(\alpha; z, s, r, D_s, D_r, D_t),$$

are given by

$$P_1^{DSR}(\alpha; z, s, r, \xi_s, \xi_r, \tau) = \tau\sqrt{\frac{1}{c(\alpha; z, s)^2} - \frac{\|\xi_s\|^2}{\tau^2}} + \tau\sqrt{\frac{1}{c(\alpha; z, r)^2} - \frac{\|\xi_r\|^2}{\tau^2}}, \tag{4.2}$$

and is solved in the direction of increasing z as before. Naturally, surface reflection data, u_0, are assumed to be independent of α. (However, one could account for α-dependent data in time-lapse seismic surveys.). Here, the solution $u(\alpha; z, s, r, t)$ corresponds with data downward continued from the surface ($z = 0$) to depth z assuming a background velocity model $c(\alpha; z, x)$.

To develop an operator for continuing $u(\alpha; z, s, r, t)$ in α, we will need $\partial_\alpha P^{DSR}$, which is still essentially a pseudodifferential operator of order 1. The principal symbol of $\partial_\alpha P^{DSR}$ is given by

$$(\partial_\alpha P^{DSR})_1(\alpha; z, s, r, \xi_s, \xi_r, \tau) = -\frac{\tau}{\sqrt{c_s^{-2} - \|\xi_s\|^2/\tau^2}} \frac{\partial_\alpha c_s}{c_s^3} - \frac{\tau}{\sqrt{c_r^{-2} - \|\xi_r\|^2/\tau^2}} \frac{\partial_\alpha c_r}{c_r^3}, \tag{4.3}$$

in which $c_s = c(\alpha; z, s)$, and $c_r = c(\alpha; z, r)$.

4.1. Evolution equation and propagator. A family of velocity models, $c(\alpha; z, x)$, induces a family of solution operators, $H^*_{(0,z)}(\alpha)$, to the initial value problems (4.1), that is, $u(\alpha; z, s, r, t) = H^*_{(0,z)}(\alpha)u_0$. Upon substituting this representation into (4.1), and taking a formal derivative with respect to α, we obtain

$$[\partial_z - \mathrm{i}P^{DSR}(\alpha)](\partial_\alpha H^*_{(0,z)}(\alpha))u_0 = \mathrm{i}(\partial_\alpha P^{DSR}(\alpha))H^*_{(0,z)}(\alpha)u_0. \tag{4.4}$$

Equation (4.4) is an inhomogeneous variant of equation (4.1) satisfied by the function $\partial_\alpha H^*_{(z,0)}(\alpha)u_0$. Its solution may be expressed in the form:

$$(\partial_\alpha H^*_{(0,z)}(\alpha)u_0)(z, .) = \mathrm{i}\left[\int_0^z H^*_{(\bar{z},z)}(\alpha)(\partial_\alpha P^{DSR}(\alpha))H^*_{(0,\bar{z})}(\alpha)\,\mathrm{d}\bar{z}\right] u_0. \tag{4.5}$$

This equation is identical to equation (C4) in [13] (but without the pseudodifferential factors Q and microlocal cutoffs ψ).

Also we can rewrite (4.5) in the form

$$\partial_\alpha H^*_{(0,z)}(\alpha)u_0 = \mathrm{i}P^d(\alpha)H^*_{(0,z)}(\alpha)u_0, \quad P^d(\alpha) = \int_0^z H^*_{(\bar{z},z)}(\alpha)(\partial_\alpha P^{DSR}(\alpha))H_{(\bar{z},z)}(\alpha)\,\mathrm{d}\bar{z}, \tag{4.6}$$

where we used the properties (3.4) and $H^*_{(0,z)}(\alpha) = H^*_{(\bar{z},z)}(\alpha)H^*_{(0,\bar{z})}(\alpha)$ with $0 < \bar{z} < z$. We note that expressions (4.5) and (4.6) provide two ways of calculating the perturbation of downward continued data $u(\alpha; z, s, r, t) = H^*_{(0,z)}(\alpha)u_0$ (at depth z) due to smooth perturbations of background velocities. Both ways are illustrated schematically in Fig. 4 (a). The evaluation of the integrand in the integral on the right-hand side of (4.5), for one fixed $\bar{z}$, is illustrated in Fig. 4 (a) left. This formulation basically mimics transmission tomography (with the DSR equation) as it uses linear perturbation theory to downward continued contributions due to smooth velocity perturbations, and add them at the depth of interest, z. It can be also associated with the concept of remigrating the data (as the computation of the integrand for each depth $\bar{z}$ initiates at the surface). The evaluation of the integrand (for one fixed $\bar{z}$) in the integral representation for $P^d(\alpha)$ (4.6) is illustrated in Fig. 4 (a) right. The scheme follows the cascading of upward and downward continuation operators. This approach fits the concept of velocity continuation as it acts on downward continued data $u(\alpha; z, s, r, t)$ while its output is again u subject to a background velocity perturbation. This description is naturally connected with reflection tomography.

According to Egorov's theorem (see Appendix A), $Q^d(\alpha; \bar{z}, z) = H^*_{(\bar{z},z)}(\alpha)(\partial_\alpha P^{DSR}(\alpha))H_{(\bar{z},z)}(\alpha)$ is a pseudodifferential operator of order 1, the principal symbol of which is obtained by the transformation (defined by the DSR rays of operator $H_{(\bar{z},z)}(\alpha)$)

$$Q^d_1(\alpha; \bar{z}, z, s, r, t, \xi_s, \xi_r, \tau) = (\partial_\alpha P^{DSR})_1(\alpha; \bar{z}, \Sigma'(\bar{z}, z)(s, r, t, \xi_s, \xi_r, \tau)), \tag{4.7}$$

with $\bar{z} < z$; the prime in Σ' indicates that the output time coordinate in Σ (cf. (3.7)) has been removed. Σ is the transformation describing upward DSR rays in phase space in velocity model $c(\alpha; z, x)$, while the explicit expression for $(\partial_\alpha P^{DSR})_1$ was given in (4.3). We obtain

$$P^d_1(\alpha; z, s, r, t, \xi_s, \xi_r, \tau) = \int_0^z Q^d_1(\alpha; \bar{z}, z, s, r, t, \xi_s, \xi_r, \tau)\,\mathrm{d}\bar{z}. \tag{4.8}$$

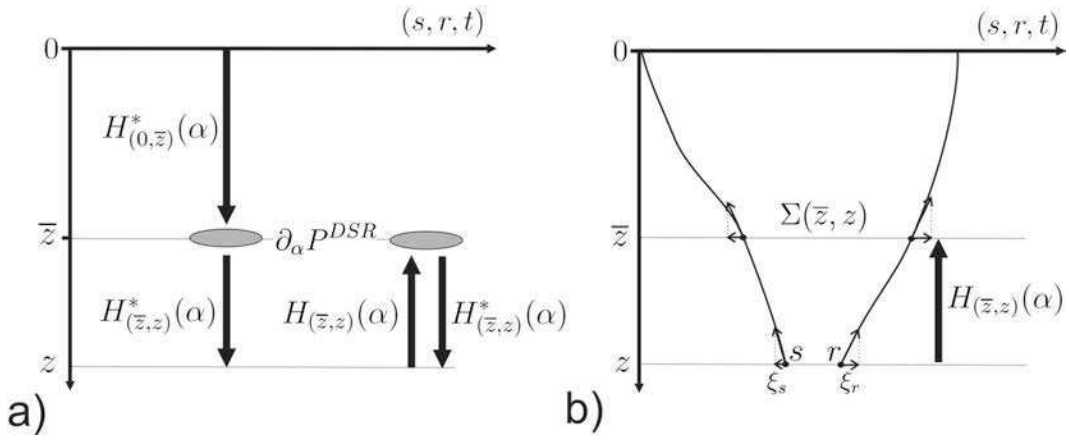

FIG. 4. *Calculation of the evolution operator for velocity continuation of downward continued data. (a) Linear perturbation due to smooth variations of the background velocity; left – as manifestation of transmission tomography (cf. (4.5)); right – as manifestation of reflection tomography (cf. (4.6)); (b) Geometry of the upward continuation operator, transformation Σ, and DSR rays.*

The variables appearing through the transformation Σ are illustrated in Fig. 4 (b). We note that, with $\xi_z = P_1^{DSR}(z, s, r, t, \xi_s, \xi_r, \tau)$, Σ also defines the DSR ray in $(z, s, r, t, \xi_z, \xi_s, \xi_r, \tau)$-space (that is a coupled pair of standard rays in source and receiver coordinates correspondingly).

The velocity continuation of $u(\alpha; z, s, r, t)$ at a given depth z is described by the continuation operator,

$$C^d_{(\alpha,\alpha_0)}(z) = H^*_{(0,z)}(\alpha) H_{(0,z)}(\alpha_0). \tag{4.9}$$

From the properties of $H_{(0,z)}(\alpha)$ [37] it indeed follows that condition (2.2) is satisfied. Then

$$u(\alpha; z, .) = C^d_{(\alpha,\alpha_0)}(z) u(\alpha_0; z, .).$$

In accordance with the theory summarized in Section 2, $C^d_{(\alpha,\alpha_0)}(z)$ is the solution operator to

$$[\partial_\alpha - \mathrm{i}P^d(\alpha)]u(\alpha; z, .) = 0, \quad u(\alpha_0; z.) = H^*_{(0,z)}(\alpha_0) u_0(.) \tag{4.10}$$

for each z (being a parameter here); the principal symbol of $P^d(\alpha)$ is given in (4.8). As before, we have assumed that the surface reflection data u_0 are independent of α. (As compared with (2.3) we have $X = (s, r, t)$; z has become a parameter.)

4.2. Continuation rays in phase space. The Hamiltonian associated with (4.10) is given by

$$\mathcal{H}^d(\alpha; z, s, r, \xi_\alpha, \xi_s, \xi_r, \tau) = \xi_\alpha - P^d_1(\alpha; z, s, r, \xi_s, \xi_r, \tau), \tag{4.11}$$

The Hamilton-Jacobi equations (cf. (2.6)) take the form

$$\frac{\mathrm{d}(s, r, t)}{\mathrm{d}\alpha} = -\frac{\partial P^d_1}{\partial(\xi_s, \xi_r, \tau)} = V_1(\alpha, z; s, r, t, \xi_s, \xi_r, \tau), \tag{4.12}$$

$$\frac{\mathrm{d}(\xi_s, \xi_r, \tau)}{\mathrm{d}\alpha} = \frac{\partial P^d_1}{\partial(s, r, t)} = V_2(\alpha, z; s, r, t, \xi_s, \xi_r, \tau),$$

in which

$$V_1(\alpha,z;.) = -\int_0^z \Big[\frac{\partial\Sigma_1(\bar z,z)}{\partial(\xi_s,\xi_r,\tau)} \frac{\partial(\partial_\alpha P^{DSR})_1}{\partial(s,r,t)}(\alpha;z,\Sigma'(\bar z,z)(.)) + \frac{\partial\Sigma_2(\bar z,z)}{\partial(\xi_s,\xi_r,\tau)} \frac{\partial(\partial_\alpha P^{DSR})_1}{\partial(\xi_s,\xi_r,\tau)}(\alpha;z,\Sigma'(\bar z,z)(.)) \Big] \,\mathrm{d}\bar z, \tag{4.13}$$

$$V_2(\alpha,z;.) = \int_0^z \Big[\frac{\partial\Sigma_1(\bar z,z)}{\partial(s,r,t)} \frac{\partial(\partial_\alpha P^{DSR})_1}{\partial(s,r,t)}(\alpha;z,\Sigma'(\bar z,z)(.)) + \frac{\partial\Sigma_2(\bar z,z)}{\partial(s,r,t)} \frac{\partial(\partial_\alpha P^{DSR})_1}{\partial(\xi_s,\xi_r,\tau)}(\alpha;z,\Sigma'(\bar z,z)(.)) \Big] \,\mathrm{d}\bar z; \tag{4.14}$$

here, the derivatives in $\frac{\partial\Sigma_{1,2}(\bar z,z)}{\partial(s,r,t)}$, $\frac{\partial\Sigma_{1,2}(\bar z,z)}{\partial(\xi_s,\xi_r,\tau)}$ follow ray perturbations (with respect to initial parameters) calculated along the unperturbed DSR rays (cf. 3.6). Indeed, we have followed a linear perturbation argument much in the spirit of ray perturbation theory [16]. Thus in order to get directions for velocity continuation rays one needs to solve the dynamic ray tracing system for the DSR rays. (This aspect of velocity continuation appeared in the work of Iversen (2006) as well.)

5. Velocity continuation and imaging.

5.1. Velocity continuation of extended images. Migration with the DSR equation is built around downward continuation of the data into the subsurface, which is followed by applying appropriate imaging conditions: Restricting for each depth the downward continued data to $t = 0$ and $s = r = x$. However, here, we are interested in applying only the first imaging condition leading to an extended image, $w_e(z,s,r)$, say (note that s and r represent *subsurface* source and receiver coordinates). This object is relevant, for example, for developing tools for migration velocity analysis; see also the next subsection.

If R_t denotes the restriction to $t = 0$, the extended image follows from the surface reflection data, u_0, as

$$w_e(\alpha;z,.) = N(\alpha)^{-1} R_t H^*_{(0,z)}(\alpha) u_0, \tag{5.1}$$

where $N(\alpha)$ is a pseudodifferential operator correcting for 'amplitudes' and illumination, using a background velocity model parametrized by α as before. (A usual image, at (z,x), is obtained by $w_e(\alpha;z,x,x)$.) We identify

$$R_t H^*_{(0,z)}(\alpha) = K^*, \tag{5.2}$$

with the adjoint of an operator K, with

$$u_0 = K(\alpha) w_e(\alpha;.) = \int_0^Z H_{(0,\bar z)}(\alpha) E_t w_e(\alpha;\bar z,.)\,\mathrm{d}\bar z, \tag{5.3}$$

while $N(\alpha) = K^*(\alpha)K(\alpha)$; here, $E_t = R_t^*$ yields a multiplication with $\delta(t)$. (Up to the differentiation $[-\frac{1}{2}\partial_t^2]$ the operator K corresponds with the depth-to-time conversion operator $\bar K$ in [37].)

The velocity continuation of an extended image is described by

$$w_e(\alpha;.) = C^e_{(\alpha,\alpha_0)} w_e(\alpha_0;.), \tag{5.4}$$

where $C^e_{(\alpha,\alpha_0)}$ denotes the relevant continuation operator. Using the depth-to-time conversion operator concept, we get

$$C^e_{(\alpha,\alpha_0)} w_e(\alpha_0;.) = N(\alpha)^{-1} K^*(\alpha) K(\alpha_0) w_e(\alpha_0;.). \tag{5.5}$$

In [37] it was established that $K = K(\alpha)$ is (microlocally) invertible. We now construct an evolution equation for $w_e(\alpha;.)$ with respect to α.

Differentiation of $C^e_{(\alpha,\alpha_0)} w_e(\alpha_0;.)$ in (5.5) with respect to α yields two terms: The term,

$$(\partial_\alpha N^{-1})(\alpha) N(\alpha) C^e_{(\alpha,\alpha_0)} w_e(\alpha_0;.),$$

is of order zero, and is neglected in the further analysis. The leading order (order one) term gives

$$\mathrm{i} N^{-1}(\alpha) \Big[\, R_t P^d(\alpha) H^*_{(0,z)}(\alpha) \, \Big] K(\alpha_0) w_e(\alpha_0;.), \tag{5.6}$$

from 5.2 upon substituting (4.6). This operator in the leading-order term can be rewritten as (using (3.4)),

$$\mathrm{i} N^{-1}(\alpha) K^*(\alpha) H_{(0,z)}(\alpha) P^d(\alpha) H^*_{(0,z)}(\alpha) K(\alpha) \, C^e_{(\alpha,\alpha_0)} = \mathrm{i} P^e(\alpha) C^e_{(\alpha,\alpha_0)}. \tag{5.7}$$

We apply Egorov's theorem twice, and find that $P^e(\alpha)$ is a pseudodifferential operator the principal symbol of which is obtained from the principal symbol of $P^d(\alpha)$ via two successive transformations of variables: The transformation associated with $H_{(0,z)}$ is $\Sigma(0,z)$ given in (3.7) with $z = 0$ and $z_1 = z$, while the transformation associated with K is given by [36, , Thm. 4.2]

$$\Sigma_K : \, (z,s,r,\xi_z,\xi_s,\xi_r) \to \Sigma(0,z)(s,r,0,\xi_s,\xi_r, \, \Theta^{-1}(z,s,r,\xi_z,\xi_s,\xi_r)), \tag{5.8}$$

where the mapping Θ solves the equation (cf. (3.5))

$$\mathcal{H}^{DSR}(z,s,r,t, \, \Theta(z,s,r,\xi_s,\xi_r,\tau),\xi_s,\xi_r,\tau) = 0$$

as before, cf. [36, , Lemma 4.1]. The composition of transformations then yields,

$$\Sigma(z,0) \circ \Sigma_K : \, (z,s,r,\xi_z,\xi_s,\xi_r) \to (s,r,0,\xi_s,\xi_r, \, \Theta^{-1}(z,s,r,\xi_z,\xi_s,\xi_r)), \tag{5.9}$$

which appears in the application of Egorov's theorem (see Appendix A) to (5.7). We get:

$$P^e_1(\alpha;z,s,r,\xi_z,\xi_s,\xi_r) = P^d_1(\alpha;z,s,r,\xi_s,\xi_r, \, \Theta^{-1}(z,s,r,\xi_z,\xi_s,\xi_r)), \tag{5.10}$$

up to principal parts. $C^e_{(\alpha,\alpha_0)}$ is the solution operator associated with the evolution equation,

$$[\partial_\alpha - \mathrm{i} P^e(\alpha)] w_e(\alpha;.) = 0. \tag{5.11}$$

(As compared with (2.3) we have $X = (z,s,r)$.) The corresponding Hamiltonian becomes

$$\mathcal{H}^e(\alpha;z,s,r,\xi_\alpha,\xi_z,\xi_s,\xi_r) = \xi_\alpha - P^e_1(\alpha;z,s,r,\xi_z,\xi_s,\xi_r). \tag{5.12}$$

In general, the evaluation of symbols $P^d_1(\alpha;z,s,r,\xi_s,\xi_r,\tau)$ and $P^e_1(\alpha;z,s,r,\xi_z,\xi_s,\xi_r)$ (cf. (5.10)) requires retracing DSR rays for each α (cf. (4.7)-(4.8)). However, in the special case of vertically inhomogeneous background velocities, this can be avoided, see Appendix B.

5.2. Velocity continuation of image gathers. Surface reflection data are, formally, redundant: The measurements are taken in $2n-1$ variables, while the image to be constructed is a function of n variables. This redundancy is revealed by the angle transform, A_{WE} [35], which generates common image-point gathers, here denoted by w_g, from surface reflection data, u_0. These common image-point gathers can be directly used in wave-equation migration velocity analysis [37, 12, 13]. Here, we consider the velocity continuation of these image gathers, with velocity models $c = c(\alpha;z,x)$ parametrized by α as before.

Let $A_{WE}(\alpha)$ denote a family of angle transforms parametrized by α; $A_{WE}(\alpha)$ is defined by

$$w_g(\alpha) = A_{WE}(\alpha) u_0 = B\chi \, H^*_{(0,z)}(\alpha) u_0, \quad \text{with} \tag{5.13}$$

$$B\chi : \, u(z,s,r,t) \to (B\chi u)(z,x,p) = \int u(z,x-h,x+h,\langle p,2h\rangle) \chi(z,x,h) \, \mathrm{d}h,$$

in which $\chi(z,x,h)$ is a taper function attaining the value 1 around $h=0$ (which ensures that the image gather is artifact free in the presence of caustics); here, (z,x) are the coordinates of an image point. (A convential common image-point gather is $w_g(\alpha;z,x,p)$ as a function of (z,p) for fixed x.) We note that p is a $(2n-1-n=n-1)$-dimensional (co)vector, and can be connected to scattering angle and azimuth associated with the geometry of reflected rays [11].

The velocity continuation of image gathers is described by

$$w_g(\alpha;z,x,p)=C^g_{(\alpha,\alpha_0)}w_g(\alpha_0;z,x,p), \tag{5.14}$$

where $C^g_{(\alpha,\alpha_0)}$ denotes the relevant continuation operator. Using that the angle transform is (microlocally) invertible [37], we have

$$C^g_{(\alpha,\alpha_0)}=A_{WE}(\alpha)A^{-1}_{WE}(\alpha_0). \tag{5.15}$$

We now construct an evolution equation for $w_g(\alpha;.)$ with respect to α.

Differentiation of $C^g_{(\alpha,\alpha_0)}w_g(\alpha_0;.)$ in (5.14) with respect to α yields

$$\partial_\alpha C^g_{(\alpha,\alpha_0)}w_g(\alpha_0;.)=\mathrm{i}B\chi\ P^d(\alpha)H^*_{(0,z)}(\alpha)A^{-1}_{WE}(\alpha_0)w_g(\alpha_0;.), \tag{5.16}$$

upon substituting (4.6). We can rewrite the composition of operators acting on $w_g(\alpha_0;.)$ on the right-hand side in the form (using (3.4))

$$\mathrm{i}A_{WE}(\alpha)H_{(0,z)}(\alpha)P^d(\alpha)H^*_{(0,z)}(\alpha)A^{-1}_{WE}(\alpha)\,C^g_{(\alpha,\alpha_0)}=\mathrm{i}P^g(\alpha)C^g_{(\alpha,\alpha_0)}. \tag{5.17}$$

We apply Egorov's theorem twice, and find that $P^g(\alpha)$ is a pseudodifferential operator the principal symbol of which is obtained from the principal symbol of $P^d(\alpha)$ via two successive transformations of variables: The transformation associated with $H^*_{(0,z)}$ is $\Sigma(z,0)$ given in (3.7) with $z_1=0$, while the transformation associated with A^{-1}_{WE} is given by

$$\Sigma^{-1}_{A_{WE}}:\ (z,x,p,\xi_z,\xi_x,\xi_p)\to\Gamma_A=(s_0,r_0,t_0,\xi_{s0},\xi_{r0},\tau),$$

where Γ_A is the solution of the system of equations [37, , Thm. 3.1]:

$$\begin{array}{rcl} P_1^{DSR}(z,s(z,0,\Gamma_A),r(z,0,\Gamma_A),\xi_s(z,0,\Gamma_A),\xi_r(z,0,\Gamma_A),\tau)\ \stackrel{*}{=}\ \xi_z & , \\ \frac{1}{2}[s(z,0,\Gamma_A)+r(z,0,\Gamma_A)]\ =\ x\quad , \quad \xi_s(z,0,\Gamma_A)\ =\ \frac{1}{2}\xi_x+\tau p & , \\ \tau[r(z,0,\Gamma_A)-s(z,0,\Gamma_A)]\ =\ \xi_p\quad , \quad \xi_r(z,0,\Gamma_A)\ =\ \frac{1}{2}\xi_x-\tau p & ; \end{array} \tag{5.18}$$

the solution is constrained by the equation

$$\tau^{-1}\,\langle\tfrac{1}{2}(\xi_s(z,0,\Gamma_A)-\xi_r(z,0,\Gamma_A)),r(z,0,\Gamma_A)-s(z,0,\Gamma_A)\rangle=t(z,0,\Gamma_A) \tag{5.19}$$

for each z. Thus we are looking for initial conditions Γ_A such that output of mapping $\Sigma(z,0)(\Gamma_A)$ (cf. (3.7)) solves the system (5.18)-(5.19). The equation labelled with $*$ can be rewritten as

$$\Theta^{-1}(z,s(z,0,\Gamma_A),r(z,0,\Gamma_A),\xi_z,\xi_s(z,0,\Gamma_A),\xi_r(z,0,\Gamma_A))=\tau. \tag{5.20}$$

The composition of the above mentioned transformations is then given by

$$\tilde{\Sigma}=\Sigma(z,0)\circ\Sigma^{-1}_{A_{WE}}:\ (z,x,p,\xi_z,\xi_x,\xi_p)\to\Sigma(z,0)(\Gamma_A)=\Gamma_B. \tag{5.21}$$

Note that Γ_A becomes implicit in this mapping and in fact the system (5.18)-(5.19) is constraining elements of $\Gamma_B=\Sigma(z,0)(\Gamma_A)$ ($s(z,0,\Gamma_A)$, etc.). Then Γ_B (in (5.21)) represents the solution to (5.18) after rearrangement (5.20)

$$\begin{array}{rcl} \frac{1}{2}[s+r] = x \quad , \quad \xi_s = \frac{1}{2}\xi_x + \Theta^{-1}(z,s,r,\xi_z,\xi_s,\xi_r)p \quad , \\ \Theta^{-1}(z,s,r,\xi_z,\xi_s,\xi_r)\,[r-s] = \xi_p \quad , \quad \xi_r = \frac{1}{2}\xi_x - \Theta^{-1}(z,s,r,\xi_z,\xi_s,\xi_r)p \quad , \end{array} \tag{5.22}$$

where $\Gamma_B = (s, r, t, \xi_s, \xi_r, \tau)$, t follows from (5.19); this guarantees proper $\Gamma_A = \Sigma(0, z)(\Gamma_B)$ (due to invertibility of mapping (3.7)).

Composition (5.21) appears in the application of Egorov's theorem (see Appendix A) to (5.17). We get:

$$P_1^g(\alpha; z, x, p, \xi_z, \xi_x, \xi_p) = P_1^d(\alpha; \tilde{\Sigma}'(z, x, p, \xi_z, \xi_x, \xi_p)); \tag{5.23}$$

as before, the prime in $\tilde{\Sigma}'$ indicates that the output time coordinate in $\tilde{\Sigma}$ (cf. (5.21)) has been removed.

$C^g_{(\alpha,\alpha_0)}$ is the solution operator associated with the evolution equation,

$$[\partial_\alpha - \mathrm{i}P^g(\alpha)]w_g(\alpha; .) = 0. \tag{5.24}$$

(As compared with (2.3) we have $X = (z, x, p)$.) The corresponding Hamiltonian becomes

$$\mathcal{H}^g(\alpha; z, x, p, \xi_\alpha, \xi_z, \xi_x, \xi_p) = \xi_\alpha - P_1^g(\alpha; z, x, p, \xi_z, \xi_x, \xi_p). \tag{5.25}$$

6. An example: Velocity continuation with a lens. In this section, we present a two-dimensional example of velocity continuation of common image-point gathers, and of an extended image. We focus on the high-frequency aspects, carry out our calculations with the relevant principal symbols, and follow the geometry of 'fronts' (singular supports to be precise). We specifically include the formation of caustics and illustrate that their presence is allowed in the approach developed here. We make use of background velocity models containing a low velocity lens:

$$c(\alpha; x, z) = 1 - \alpha \exp[-7.5(x^2 + (1 - z)^2)], \tag{6.1}$$

where α defines the 'strength' of the lens. We take $\alpha = 0.2$ as our 'true' model (see Fig. 5 (a), where the smooth background velocity (low-velocity lens) is shown in grey scale). We consider a single, horizontal, reflector (solid line) at depth $z = 2$. Synthetic data, u_0 (traveltimes, as we consider only geometry), were generated in the 'true' model by methods of ray tracing. In Fig. 6 we show incident (a) and reflected (b) rays for one source position, to illustrate that in our example the DSR condition is satisfied, while caustics are being formed due to the lens.

In Fig. 5 (b) we show a common image-point gather (its singular support) $w_g(\alpha = 0.2; z, x, p)$ (cf. (5.13)) if the 'true' background velocity model were used in the downward continuation. The reflector (the horizontal line in Fig. 5 (a)) is mapped into a plane (Fig. 5 (b), in grey). A common image-point gather is usually associated with an x =const section (line 2); a constant p section corresponds to an image (line 1).

The evolution of a 'front' of $w_g(\alpha; z, x, p)$ with α is illustrated in Fig. 7 (a) (top: $\alpha = 0.2$, that is the 'true' model; middle: $\alpha = 0.1$; and bottom: $\alpha = 0$, that is, the lens is absent). Due to restricted acquisition geometry (the sources and receivers are located within an interval $(-2, 2)$) we have illumination over a diamond shaped region only (see Fig. 7 (a), (b) top). The dots in Fig. 7 (b) top indicate the initial locations of a set of velocity continuation rays; the dots in Fig. 7 (b) middle, bottom, indicate the points (at $\alpha = 0.1$ and $\alpha = 0$, respectively) of the continuation rays in this set, projected onto the (x, p) coordinate plane. We observe how the regularly spaced initial points evolve under velocity continuation, and their movement is not restricted to any coordinate plane. Indeed, migration velocity analysis should not be carried out with separated common image-point gathers.

However, due to the (common) symmetry of the background velocity models in our example, the velocity continuation appears to be 2D (velocity rays stay in the same plane) for two planes of our (z, x, p)-space, namely, $x = 0$ and $p = 0$, which are illustrated in Fig. 8. We show the 'fronts' (their sections) as thick lines, again, at $\alpha = 0.2$, 0.1 and 0 as well as the continuation (velocity) rays connecting them. Continuation in Fig. 8 (left) takes place in $p = 0$ and can be associated with conventional image; we notice the evolution towards an apparent structure of a syncline while underestimating the strength of the low velocity lens (a phenomenon that has been well recognized in seismic migration). Continuation in the plane $x = 0$ is shown in Fig. 8 (right). It corresponds with a standard common image-point gather.

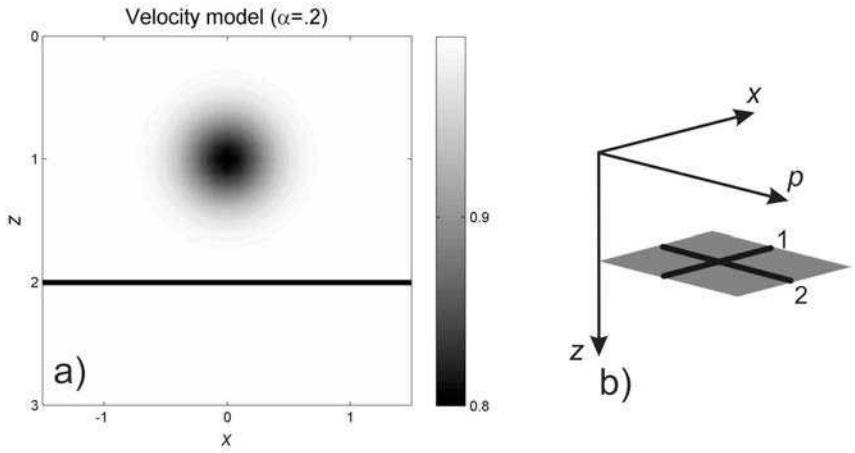

FIG. 5. *(a) The 'true' background velocity model (a low-velocity lens) and reflectivity function (reflector at $z = 2$); (b) Diagram illustrating the presence of the reflector in the common image-point gather $w_g = w_g(\alpha; z, x, p)$.*

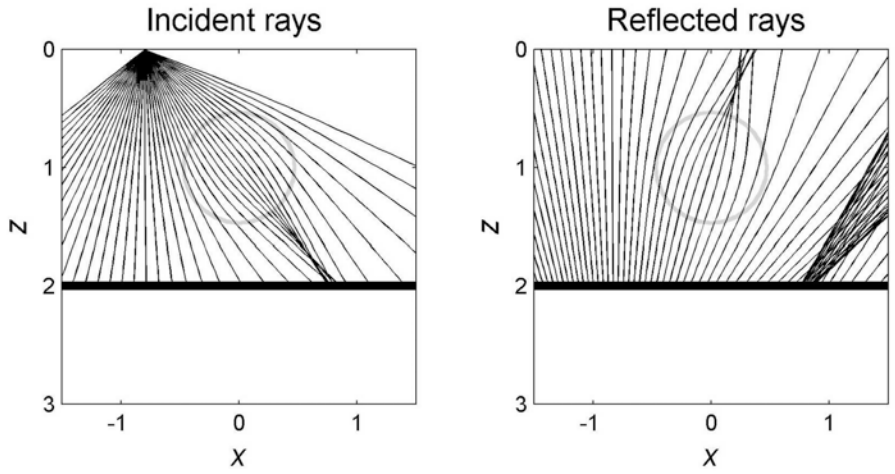

FIG. 6. *Incident and reflected rays for a single source. The lens in Fig. 5 (a) is, here, indicated by a grey circle. The rays are nowhere horizontal, while caustics are being formed.*

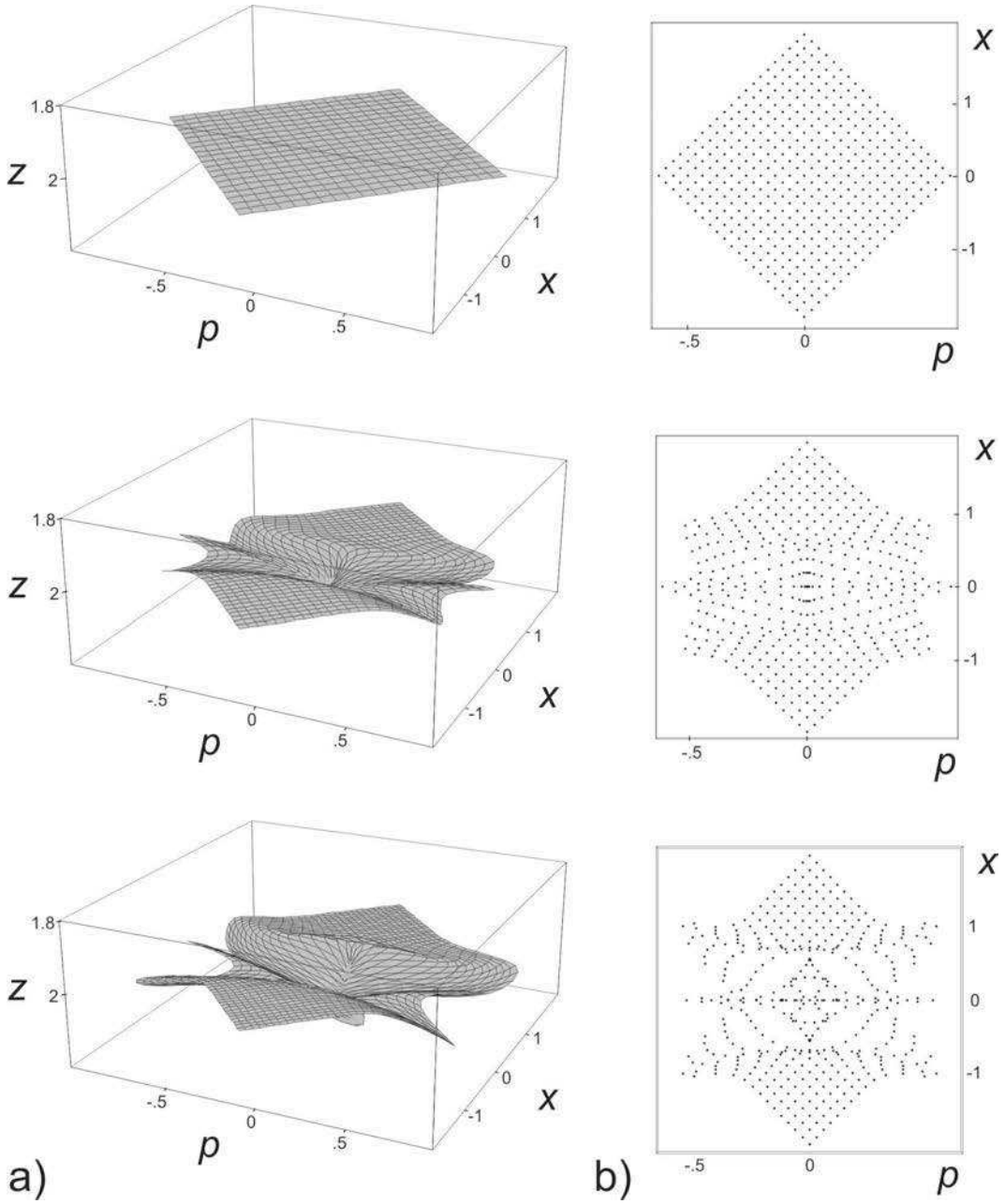

FIG. 7. *Velocity continuation of $w_g(\alpha; z, x, p)$, tracking the 'front' associated with the horizontal reflector shown in Fig. 5 (a). (a) Continuation of the grey plane of Fig. 5 (b), at $\alpha = 0.2$ (top), 0.1 (middle) and 0 (bottom); (b) A set of points on continuation rays corresponding to initial locations (top), $\alpha = 0.1$ (middle) and $\alpha = 0$ (bottom).*

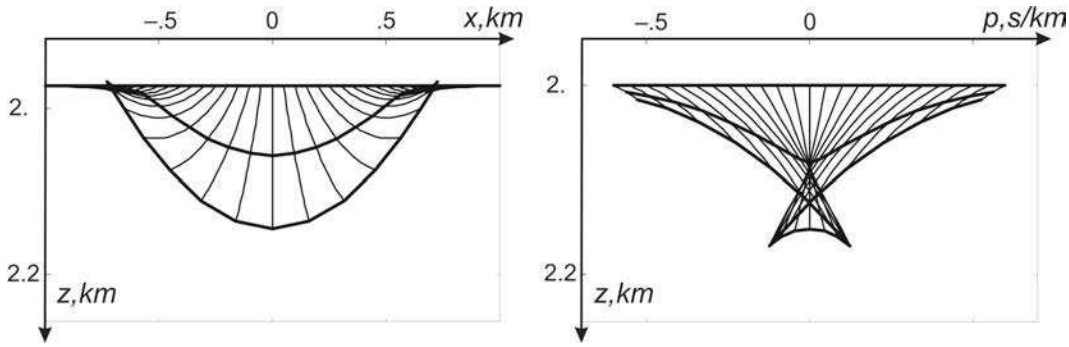

FIG. 8. *Continuation rays (thin lines) and 'fronts' at $\alpha = 0.2,\ 0.1$ and 0 (fat lines) under velocity continuation in the $p = 0$ (image) plane (left) and the $x = 0$ (image gather) plane (right). These are sections of the volumes illustrated in Fig. 7.*

We then use the some background model and reflector to illustrate velocity continuation of the extended image $w_e(\alpha; z, x, h)$. In the 'true' model, the extended image is a line focused in (z, x, h)-space at subsurface offset $h = 0$. This line defocuses, while departing from the 'true' background model, following the fronts shown in Fig. 9.

7. Evolution operators in homogeneous velocity models. In homogeneous velocity models ($c(z, x) = v$ independent of z and x) the evolution parameter becomes the velocity itself, $\alpha \equiv v$. The (principal) symbol of the DSR operator in (4.2) takes the form

$$P_1^{DSR}(v; z, s, r, \xi_s, \xi_r, \tau) = \tau\sqrt{\frac{1}{v^2} - \frac{\|\xi_s\|^2}{\tau^2}} + \tau\sqrt{\frac{1}{v^2} - \frac{\|\xi_r\|^2}{\tau^2}}, \tag{7.1}$$

while the (principal) symbol in (4.3) becomes

$$\begin{aligned}(\partial_v P^{DSR})_1(v; z, s, r, \xi_s, \xi_r, \tau) &= -\frac{\tau}{\sqrt{v^{-2} - \|\xi_s\|^2/\tau^2}}\frac{1}{v^3} - \frac{\tau}{\sqrt{v^{-2} - \|\xi_r\|^2/\tau^2}}\frac{1}{v^3} \\ &= -\frac{1}{v^3}\frac{\xi_z}{\sqrt{v^{-2} - \|\xi_s\|^2/\tau^2}\sqrt{v^{-2} - \|\xi_r\|^2/\tau^2}},\end{aligned} \tag{7.2}$$

using that $\mathcal{H}^{DSR}(z, s, r, t, \xi_z, \xi_s, \xi_r, \tau) = 0$, cf. (3.5). We derive, here, closed-form expressions for the evolution operators for velocity continuation of downward continued data, velocity continuation of extended images, and velocity continuation of common image-point gathers. We use these expressions to illustrate some of the features of these types of continuation that coexist in the data-extended-image volume.

Continuation of downward continued data. For the DSR rays corresponding to upward continuation operator $H_{(\bar{z},z)}(v)$, we have

$$\Sigma_2(\bar{z}, z)(s, r, t, \xi_s, \xi_r, \tau) = (\xi_s, \xi_r, \tau),$$

that is, the wave numbers are preserved, which implies, with (7.2), that $(\partial_\alpha P^{DSR})_1(v; \bar{z}, \Sigma'(\bar{z}, z)(s, r, t, \xi_s, \xi_r, \tau))$ (cf. (4.7)) is independent of $\bar{z}$. Evaluation of (4.8) then yields

$$P_1^d(v; z, s, r, \xi_s, \xi_r, \tau) = -\frac{\tau\, z}{v^3}\left(\frac{1}{\sqrt{v^{-2} - \|\xi_s\|^2/\tau^2}} + \frac{1}{\sqrt{v^{-2} - \|\xi_r\|^2/\tau^2}}\right). \tag{7.3}$$

Extended image continuation. We get $\tau = \Theta^{-1}(v; z, s, r, \xi_z, \xi_s, \xi_r)$ directly from the equation, $\mathcal{H}^{TWT}(s, r, z, \tau, \xi_s, \xi_r, \xi_z) = 0$, using (3.21) subject to the substitution $c(z) = v$, and note that with the solution $\tau = \tau(v; z, s, r, \xi_z, \xi_s, \xi_r)$,

(7.4)

$$\tau\sqrt{v^{-2} - \|\xi_s\|^2/\tau^2} = \frac{1}{2\xi_z}\left(\xi_z^2 + \|\xi_r\|^2 - \|\xi_s\|^2\right),\ \tau\sqrt{v^{-2} - \|\xi_r\|^2/\tau^2} = \frac{1}{2\xi_z}\left(\xi_z^2 + \|\xi_s\|^2 - \|\xi_r\|^2\right).$$

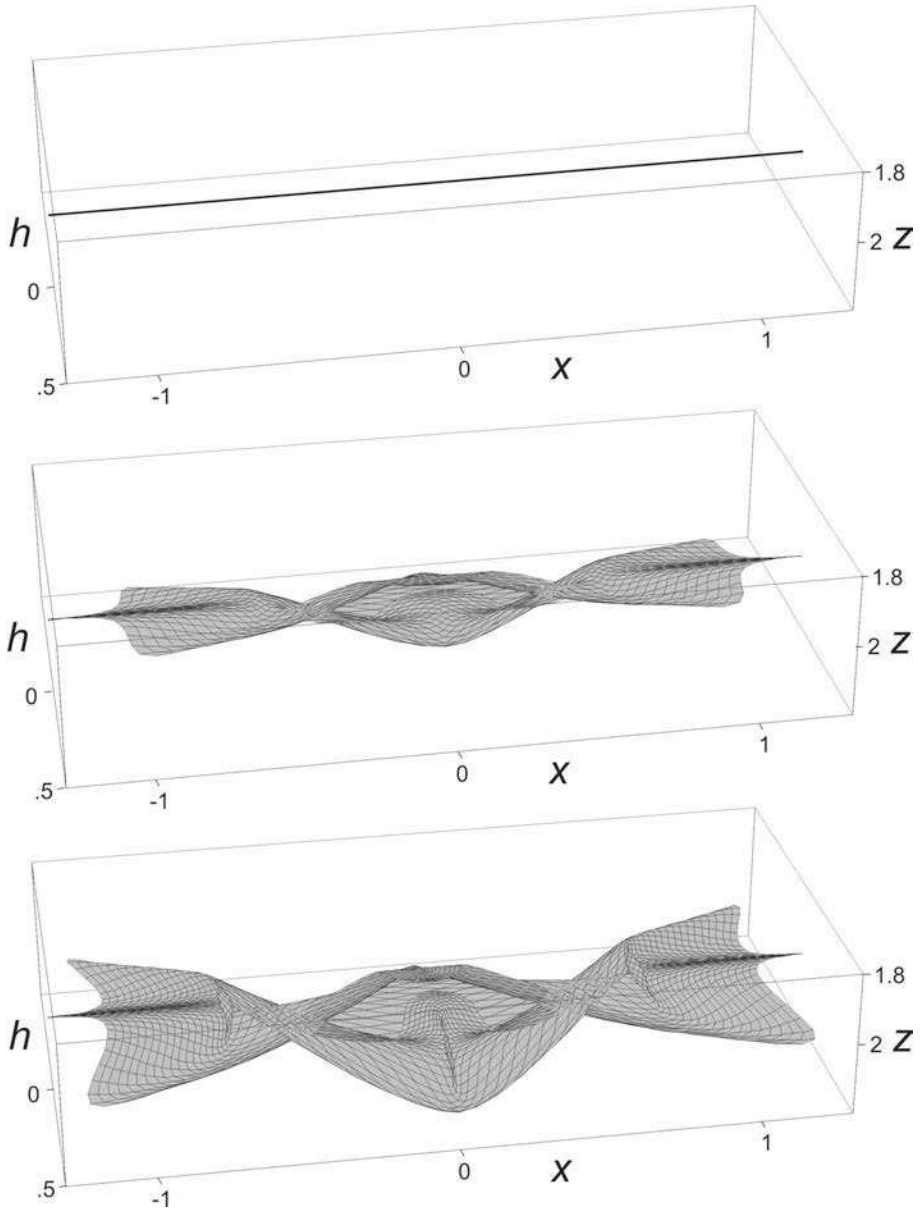

FIG. 9. *Velocity continuation of the extended image $w_e(\alpha; z, x, h)$, tracking the 'front' associated with the horizontal reflector shown in Fig. 5 (a): at $\alpha = 0.2$ (a line representing the focusing at $h = 0$), 0.1 and 0, signifying the gradual defocusing.*

Then, with (7.3) and (7.4), the evaluation of (5.10) yields

$$P_1^e(v; z, s, r, \xi_z, \xi_s, \xi_r) = -\frac{z}{v}\xi_z \frac{\xi_z^4 + 2\xi_z^2(\|\xi_r\|^2 + \|\xi_s\|^2) + (\|\xi_s\|^2 - \|\xi_r\|^2)^2}{\xi_z^4 - (\|\xi_s\|^2 - \|\xi_r\|^2)^2}. \tag{7.5}$$

Applying coordinate transformation (3.10) results in

$$P_1^e(v; z, x, h, \xi_z, \xi_x, \xi_h) = -\frac{z}{v}\xi_z \frac{\xi_z^4 + \xi_z^2(\|\xi_x\|^2 + \|\xi_h\|^2) + \langle \xi_x, \xi_h \rangle^2}{\xi_z^4 - \langle \xi_x, \xi_h \rangle^2}. \tag{7.6}$$

REMARK (Stolt residual migration). Given the (principal) symbol, P_1^e, for extended image continuation, we obtain the Hamiltonian (cf. (2.5))

$$\mathcal{H}^e(v;z,s,r,\xi_v,\xi_z,\xi_s,\xi_r) = \xi_v - P_1^e(v;z,s,r,\xi_z,\xi_s,\xi_r), \tag{7.7}$$

which generates corresponding Hamilton-Jacobi equations (2.6). With (7.5), these equations can be solved explicitly for given initial conditions $(z_0, s_0, r_0, \xi_{z0}, \xi_{s0}, \xi_{r0})$ (at $v = v_0$ say), resulting directly in the formulas for Stolt residual migration (see [31, 38]). Note, however, that our Hamiltonian representation (7.5)-(7.6) is general, and allows different implementations in addition to the phase shift method (as discussed in [20]).

Continuation of common image-point gathers. In homogeneous background velocity models, the symbol P_1^{DSR} is independent of s and r, whence the equations for (ξ_s, ξ_r, τ) in (5.22),(5.20), given (ξ_z, ξ_x, ξ_p), can be solved separately:

$$\xi_s = \tfrac{1}{2}\xi_x + \tau p, \quad \xi_r = \tfrac{1}{2}\xi_x - \tau p, \quad \text{with } \tau^2 = \frac{\xi_z^2 v^2}{4}\frac{\xi_z^2 + \|\xi_x\|^2}{\xi_z^2(1-\|vp\|^2) - \langle \xi_x, vp\rangle^2}; \tag{7.8}$$

these are all preserved under $\Sigma(z,0)$. We then use the equations for (s,r) in (5.22), given (x,ξ_p), to find s and r:

$$s = x - \frac{\xi_p}{2\tau}, \quad r = x + \frac{\xi_p}{2\tau}. \tag{7.9}$$

Equation (5.19) yields

$$t = \tau^{-1}\langle p, \xi_p\rangle. \tag{7.10}$$

We immediately have obtained transformation $\tilde{\Sigma}$ in (5.21). Subjecting (7.3) to this transformation then yields

$$P_1^g(v;z,x,p,\xi_z,\xi_x,\xi_p) = -\frac{z}{v}\xi_z^3\frac{\xi_z^2 + \|\xi_x\|^2}{\xi_z^4 - \|\xi_z^2 vp + \langle \xi_x, vp\rangle \xi_x\|^2}. \tag{7.11}$$

We obtain the Hamiltonian (cf. (2.5))

$$\mathcal{H}^g(v;z,x,p,\xi_v,\xi_z,\xi_x,\xi_p) = \xi_v - P_1^g(v;z,x,p,\xi_z,\xi_x,\xi_p), \tag{7.12}$$

which generates corresponding Hamilton-Jacobi equations (2.6). The Hamiltonian for common image-point gathers velocity continuation depends on (z,p) and v. In Fig. 10 (a) we show the corresponding slowness surface, defined by $\mathcal{H}^g = 0$, using the notation $k_x = \xi_x/\xi_v$, $k_z = \xi_z/\xi_v$ and $k_p = \xi_p/\xi_v$. We set $z = 2$, $v = 1$ and take two values for p: $p = 0$ (outer surface) and $p = 0.3$ (inner surface). From (7.11)-(7.12) it is clear that the slowness surface does not depend on ξ_p. This, in turn, means that the group velocity has no component in the direction of the p-axis, that is, the energy flow, in the case of homogeneous media, stays within planes $p = $ const. To illustrate this, we show a set of velocity rays in Fig. 10 (b). Here, we assume that initial common image-point gather consists of a dipping plane in (z,x,p)-space (in grey). We then follow a transformation of one straight line in his plane ($x = z = 1$) under velocity continuation. Thin lines show velocity rays, while the velocity is changing from a starting value $v = 1$ to $v = 1.2$. Three bold lines show the evolution of the straight line in the initial common image-point gather (for $v = 1$) after velocity continuation to $v = 1.1$ and $v = 1.2$.

8. Discussion. We developed a general framework for velocity continuation in the downward continuation approach to seismic imaging. We based the framework on the double-square-root (DSR) equation, and imposed the DSR assumption. In the process, it was then natural to introduce the concept of data-extended-image domain that is (z,s,r,t)-space. Continuation takes place along curves in the space of allowable velocity models. As the main result, we obtained evolution equations for three interconnected velocity continuations: for downward continued data, (extended) images and common image-point gathers formed from these. We used techniques from microlocal analysis, in particular, Egorov's theorem.

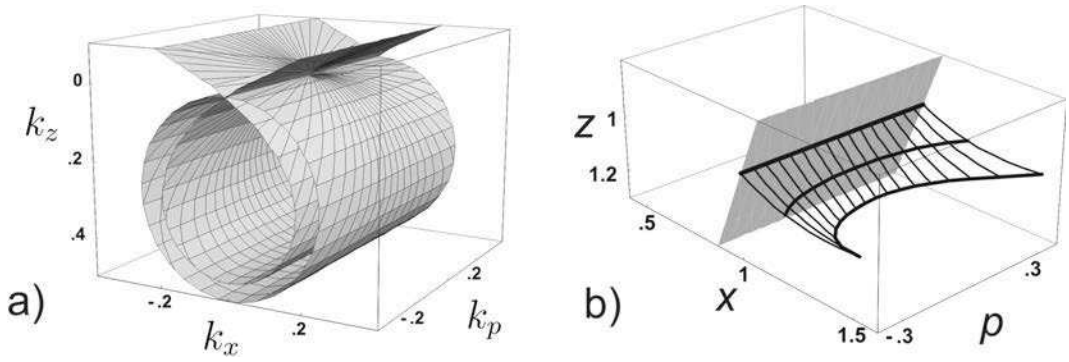

FIG. 10. *Velocity continuation of a common-image point gather in the case of homogeneous background velocities. (a) Slowness surface for the Hamiltonian in (7.12) for $v = 1$ and $p = 0$ (outer surface) and $p = 0.3$ (inner surface); (b) velocity continuation of a line in a common image-point gather consisting of a dipping plane (in grey). Thin lines represent velocity rays, while the velocity is changing from a starting value $v = 1$ to $v = 1.2$. Three bold lines show the evolution of the straight line in the initial common image-point gather (for $v = 1$) after velocity continuation to $v = 1.1$ and $v = 1.2$.*

We developed the realization of velocity continuation explicitly on the level of principal (high-frequency) symbols of the above mentioned evolution operators. The evaluation of these symbols essentially requires retracing DSR rays in the evolving velocity models. However, the downward continuation of data needs not be repeated, which enhances efficiency of operations in velocity analysis. Indeed, the data themselves are not involved in the process of velocity continuation proper.

Continuation operators are the solution operators of the above mentioned evolution equations. In general these equations need to be solved numerically, after the evolution operator symbol has been evaluated with 'retracing' DSR rays (sensing the background model variation) in phase space. Continuation operators propagate singularities along continuation rays, which are generated by Hamilton systems. Numerically solving these systems, in general, consists of two nested steps: Computing the Hamiltonians (and their derivatives), which involves a depth integration, followed by integrating the Hamilton systems. The complexity of numerically computing other continuation rays was recognized by [24, 25, 1].

The numerical solution of the evolution equation for continuation can be constructed as follows. The initial values (downward continued data, image, or image gathers) can be decomposed into curvelets or wave packets and subsequently compressed. Then the solution of the evolution can be efficiently computed with curvelets (see [4]); to leading order, the curvelets that appear in the decomposition of the initial values are subjected to a 'flow-out' [14] following the continuation 'rays' in phase space. Continuation can be viewed as an alternative to (map) remigrating curvelets that appear in the decomposition of surface reflection data [14].

We hasten to mention that in particular classes of velocity models, admitting dependence in depth only, the retracing of DSR rays is unnecessary. (This is also true, for example, in velocity continuation through so-called common reflection-point (CRP) stacks [5], using a class of velocity model perturbations, $c(\alpha; z, x) = \alpha c_0(z, x)$. Indeed, to obtain the CRP stacks, the ray geometry can be kept the same then, but the Kirchhoff summation has to be repeated for every α. In these factorizable velocity models, 'approximate' formulas for residual pre-stack Stolt migration, which naturally avoids Kirchhoff resummation, were developed and applied by [32].)

While developing velocity continuation in the downward continuation approach to seismic imaging, we show how the conventional exploding reflectors model fits in our framework, and that our results can be viewed as a generalization of residual migration. Furthermore, we extend the notion of isochron rays [24].

We derived explicit formulas for the evolution operators in the case of special background velocity models: In the case of models with a linear velocity growth with depth (the evolution parameter is the gradient) for the continuation of extended images, and in the case of homogeneous velocity models (the evolution parameter is the velocity itself) for the continuation of extended images and common image-point gathers. The latter results relate to earlier work by [19, 21]. Though not applicable to generic situations, these

formulas provide some insight also in connection with the history of residual velocity (poststack) migration (e.g. [38]).

We present a two-dimensional synthetic data example for the velocity continuation of the extended image and common image-point gathers associated with a plane horizontal reflector in a family of background models with a low-velocity lens that varies in strength. Thus we illustrate velocity continuation in the presence of caustics, and demonstrate that, in the process, image gathers cannot be separated from one another.

Acknowledgements. This research was funded in part by NSF CMG grant EAR-0417891. The authors also thank the members, ExxonMobil, Total, BP and Statoil, of the Geo-Mathematical Imaging Group for financial support.

Appendix A. Egorov's theorem.

A precise formulation of Egorov's theorem can be found in [40, , Thm. 6.2]. Here, we provide an intuitive understanding of this theorem with a view to applications in seismic wave-equation imaging.

We consider an invertible Fourier integral operator, F say, the canonical relation of which is the graph of a transformation Σ. Suppose $F:\ \mathcal{E}'(Y)\rightarrow\mathcal{D}'(X)$; F propagates singularities according to $(y,\eta)\rightarrow(x,\xi)=\Sigma(y,\eta)$. An example is F^{-1} being common-offset Kirchhoff migration (absence of caustics) and Σ describing map demigration.

We then consider a pseudodifferential operator, P, with principal symbol $P_1=P_1(x,\xi)$. The operator $Q=F^{-1}PF$ is also a pseudodifferential operator. Its principal symbol, $Q_1=Q_1(y,\eta)$, is given by a change of coordinates in P_1:

$$Q_1(y,\eta)=P_1(\Sigma(y,\eta)). \tag{A.1}$$

In the main text, we repeatedly prepare constructions for application of this theorem.

Appendix B. Vertically inhomogeneous background velocity models.

Retracing rays and perturbation theory *are not required* for velocity continuation in the case of a family of vertically inhomogeneous background velocities, $c(\alpha;z)$. Then $\mathcal{H}^{DSR}$ does not depend on s, r (and t) so that $\partial_{(s,r,t)}\mathcal{H}^{DSR}=0$ and ξ_s, ξ_r and τ are constant along DSR rays in phase space. Formulas (4.3) and (4.8) simplify according to

(B.1)
$$(\partial_\alpha P^{DSR})_1(\alpha;z,s,r,\xi_s,\xi_r,\tau)=-\frac{\partial_\alpha c}{c^3}(\alpha;z)\left[\frac{\tau}{\sqrt{c(\alpha;z)^{-2}-\|\xi_s\|^2/\tau^2}}+\frac{\tau}{\sqrt{c(\alpha;z)^{-2}-\|\xi_r\|^2/\tau^2}}\right],$$

and

(B.2)
$$P_1^d(\alpha;z,s,r,\xi_s,\xi_r,\tau)=-\int_0^z\frac{\partial_\alpha c}{c^3}(\alpha;\bar z)\left[\frac{\tau}{\sqrt{c(\alpha;\bar z)^{-2}-\|\xi_s\|^2/\tau^2}}+\frac{\tau}{\sqrt{c(\alpha;\bar z)^{-2}-\|\xi_r\|^2/\tau^2}}\right]\mathrm{d}\bar z,$$

respectively. Moreover, we obtain

$$\Theta^{-1}(z,s,r,\xi_z,\xi_s,\xi_r)=\frac{c(\alpha;z)}{2\xi_z}\sqrt{[(\|\xi_s\|-\|\xi_r\|)^2+\xi_z^2]\,[(\|\xi_s\|+\|\xi_r\|)^2+\xi_z^2]}, \tag{B.3}$$

which, upon substitution for τ in (B.2), gives us $P_1^e(\alpha;z,s,r,\xi_z,\xi_s,\xi_r)$ for velocity continuation of extended images, cf. (5.10). Clearly, no DSR rays have to be traced.

For some particular choices of families $c(\alpha;z)$, it is possible to carry out the integration on the right-hand side of (B.2) in closed form. For example, if $c(\alpha;z)=c_0+\alpha z$, we get:

(B.4)
$$P_1^d(\alpha;z,s,r,\xi_s,\xi_r,\tau)$$
$$=-\left\{\frac{1}{\alpha^2}\,c_0(q_s+q_r)-\frac{\tau}{\alpha^2}\log\left[4\alpha^4\left(q_s+\frac{\tau}{c_0+\alpha\bar z}\right)\left(q_r+\frac{\tau}{c_0+\alpha\bar z}\right)\right]\right\}_{\bar z=0}^{\bar z=z},$$

where $q_r=\tau\sqrt{(c_0+\alpha\bar z)^{-2}-\|\xi_r\|^2/\tau^2}$, $q_s=\tau\sqrt{(c_0+\alpha\bar z)^{-2}-\|\xi_s\|^2/\tau^2}$.

REFERENCES

[1] F. ADLER, *Kirchhoff image propagation*, Geophysics, 67 (2002), pp. 126–134.
[2] T. ALKHALIFAH AND M.V. DE HOOP, *Integral DMO in anisotropic media*, 66th Annual International Meeting: Expanded Abstracts, SEG, (1996), pp. 491–494.
[3] ———, *Residual dip moveout in VTI media*, Geophys. Prosp., 53 (2005), pp. 1–12.
[4] F. ANDERSSON, M.V. DE HOOP, H.F. SMITH, AND G. UHLMANN, *A multi-scale approach to hyperbolic evolution equations with limited smoothness*, Communications in Partial Differential Equations, in print (2008).
[5] F. AUDEBERT, J.P. DIET, P. GUILLAUME, I. F. JONES, AND X. ZHANG, *CRP-scans: 3-D preSDM velocity analysis via zero-offset tomographic inversion*, 67th Annual International Meeting: Expanded Abstracts, SEG, (1997), pp. 1805–1808.
[6] A.V. BELONOSOVA AND A.S. ALEKSEEV, *About one formulation of the inverse kinematic problem of seismics for a two-dimensional continuously heterogeneous medium*, in Some methods and algorithms for interpretation of geophysical data (in Russian), Nauka, 1967, pp. 137–154.
[7] G. CHENG AND S. COEN, *The relationship between Born inversion and migration of common-midpoint stacked data*, Geophysics, 49 (1984), pp. 2117–2131.
[8] J.F. CLAERBOUT, *Imaging the earth's interior*, Blackwell Scientific Publishing, Oxford, 1985.
[9] R.W. CLAYTON, *Common midpoint migration*, Technical Report, Stanford University, SEP-14 (1978).
[10] C.G.M. DE BRUIN, C.P.A. WAPENAAR, AND A.J. BERKHOUT, *Angle-dependent reflectivity by means of prestack migration*, Geophysics, 55 (1990), pp. 1223–1234.
[11] M.V. DE HOOP, J.H. LE ROUSSEAU, AND B. BIONDI, *Symplectic structure of wave-equation imaging: A path-integral approach based on the double-square-root equation*, Geoph. J. Int., 153 (2003), pp. 52–74.
[12] M.V. DE HOOP AND R.D. VAN DER HILST, *Global wave-equation reflection tomography*, Center for Wave Phenomena Preprint, 453 (2003).
[13] M.V. DE HOOP, R.D. VAN DER HILST, AND P. SHEN, *Wave-equation reflection tomography: Annihilators and sensitivity kernels*, Geoph. J. Int., 167 (2006), pp. 1332–1352.
[14] H. DOUMA AND M.V. DE HOOP, *Leading-order seismic imaging using curvelets*, Geophysics, 72 (2007), pp. S231–S248.
[15] A.A. DUCHKOV, M.V. DE HOOP, AND A. SÁ BARRETO, *Evolution-equation approach to seismic image, and data, continuation*, Wave Motion, submitted (2007).
[16] V. FARRA, *Computation of second-order traveltime perturbation by Hamiltonian ray theory*, Gephys. J. Int., 136 (1999), pp. 205–217.
[17] L. FISHMAN AND J.J. MCCOY, *Derivation and application of extended parabolic wave theories I. The factorized Helmholtz equation*, J. Math. Phys., 25 (1984), pp. 285–296.
[18] ———, *Derivation and application of extended parabolic wave theories II. Path integral representations*, J. Math. Phys., 25 (1984), pp. 297–308.
[19] S.B. FOMEL, *Method of velocity continuation in the problem of seismic time migration*, Russian Geology and Geophysics, 35, No. 5 (1994), pp. 100–111.
[20] S. FOMEL, *Time-migration velocity analysis by velocity continuation*, Geophysics, 68 (2003), pp. 1662–1672.
[21] ———, *Velocity continuation and the anatomy of residual prestack time migration*, Geophysics, 68 (2003), pp. 1650–1661.
[22] D.J. FOSTER, C.C. MOSHER, AND S. JIN, *Offset plane wave migration*, in Expanded Abstracts, Eur. Assoc. Expl. Geophys., 2002, pp. B–14.
[23] P. HUBRAL, M. TYGEL, AND J. SCHLEICHER, *Seismic image waves*, Geophys. J. Int., 125 (1996), pp. 431–442.
[24] E. IVERSEN, *The isochron ray in seismic modeling and imaging*, Geophysics, 69 (2004), pp. 1053–1070.
[25] ———, *Velocity rays for heterogeneous anisotropic media: Theory and implementation*, Geophysics, 71 (2006), pp. T117–T127.
[26] J.H. LE ROUSSEAU AND M.V. DE HOOP, *Modeling and imaging with the scalar generalized-screen algorithms in isotropic media*, Geophysics, 66 (2001), pp. 1551–1568.
[27] Z. LIU AND N. BLEISTEIN, *Migration velocity analysis: Theory and an iterative algorithm*, Geophysics, 60 (1995), pp. 142–153.
[28] I. LORIS, G. NOLET, I. DAUBECHIES, AND F.A. DAHLEN, *Tomographic inversion using ℓ^1-norm regularization of wavelet coefficients*, Geophys. J. Int., 170 (2007), pp. 359–370.
[29] Z. MENG, *Tetrahedral based earth models, ray tracing in tetrahedral models and analytical migration velocity analysis*, PhD thesis, Colorado School of Mines, 1999.
[30] C.C. MOSHER, D.J. FOSTER, AND S. HASSANZADEH, *Seismic imaging with offset plane waves*, in Mathematical Methods in Geophysical Imaging IV, Proceedings of SPIE – Volume 2822, 1996, pp. 52–63.
[31] P. SAVA, *Prestack residual migration in the frequency domain*, Geophysics, 68 (2003), pp. 634–640.
[32] P. SAVA AND B. BIONDI, *Wave-equation migration velocity analysis. I. Theory*, Geophysical Prospecting, 52 (2004), pp. 593–606.
[33] P. SHEN, *Automatic wave equation migration velocity analysis using differential semblance*, PhD thesis, Rice University, 2004.
[34] M. A. SHUBIN, *Pseudodifferential operators and spectral theory*, Springer, Berlin, New York, 2001.
[35] C.C. STOLK AND M.V. DE HOOP, *Seismic inverse scattering in the 'wave-equation' approach*, MSRI preprint, #2001–047 (2001).
[36] ———, *Modeling of seismic data in the downward continuation approach*, SIAM J. Appl. Math., 65 (2005), pp. 1388–1406.
[37] ———, *Seismic inverse scattering in the downward continuation approach*, Wave Motion, 43 (2006), pp. 579–598.
[38] R.H. STOLT, *Short note - A prestack residual time migration operator*, Geophysics, 61 (1996), pp. 605–607.
[39] W.W. SYMES AND J. CARAZZONE, *Velocity inversion by differential semblance optimization*, Geophysics, 56 (1991), pp. 654–663.
[40] F. TREVES, *Introduction to Pseudodifferential and Fourier Integral Operators*, vol. 2, Plenum Press, New York, 1980.